Human embryonic stem cell–derived cardiomyocytes restore function in infarcted hearts of non-human primates

Yen-Wen Liu[1–3,12,13], Billy Chen[1,2,4,13], Xiulan Yang[1,2,5,13], James A Fugate[1,2,5], Faith A Kalucki[1,2,5], Akiko Futakuchi-Tsuchida[1,2,5], Larry Couture[6,12], Keith W Vogel[7], Clifford A Astley[7], Audrey Baldessari[7], Jason Ogle[7], Creighton W Don[4], Zachary L Steinberg[4], Stephen P Seslar[4,8], Stephanie A Tuck[1,2,5,12], Hiroshi Tsuchida[1,2,5], Anna V Naumova[1,2,9,10], Sarah K Dupras[1,2,5], Milly S Lyu[9], James Lee[4], Dale W Hailey[1], Hans Reinecke[1,2,5], Lil Pabon[1,2,5], Benjamin H Fryer[1,2,5], W Robb MacLellan[1,2,4], R Scott Thies[1,2,5] & Charles E Murry[1,2,4,5,11]

Pluripotent stem cell–derived cardiomyocyte grafts can remuscularize substantial amounts of infarcted myocardium and beat in synchrony with the heart, but in some settings cause ventricular arrhythmias. It is unknown whether human cardiomyocytes can restore cardiac function in a physiologically relevant large animal model. Here we show that transplantation of ~750 million cryopreserved human embryonic stem cell–derived cardiomyocytes (hESC-CMs) enhances cardiac function in macaque monkeys with large myocardial infarctions. One month after hESC-CM transplantation, global left ventricular ejection fraction improved $10.6 \pm 0.9\%$ vs. $2.5 \pm 0.8\%$ in controls, and by 3 months there was an additional 12.4% improvement in treated vs. a 3.5% decline in controls. Grafts averaged 11.6% of infarct size, formed electromechanical junctions with the host heart, and by 3 months contained ~99% ventricular myocytes. A subset of animals experienced graft-associated ventricular arrhythmias, shown by electrical mapping to originate from a point-source acting as an ectopic pacemaker. Our data demonstrate that remuscularization of the infarcted macaque heart with human myocardium provides durable improvement in left ventricular function.

Heart disease kills more people worldwide than any other illness[1]. Much of this morbidity and mortality occurs because the heart is one of the least regenerative organs in the human body[2]. The ability of cardiomyocytes to proliferate is limited to ~1% per year[3–5], and it has been difficult to identify a cardiac stem cell population that can give rise to new myocytes at significant levels[3,6]. As a result, cardiac injuries, such as myocardial infarctions, heal by scar formation, and the heart loses contractile ability in direct relation to the muscle deficit. When significant myocardial mass is lost, patients often progress to heart failure. Drug treatments for heart failure manage symptoms but do not address the root problem of muscle deficiency.
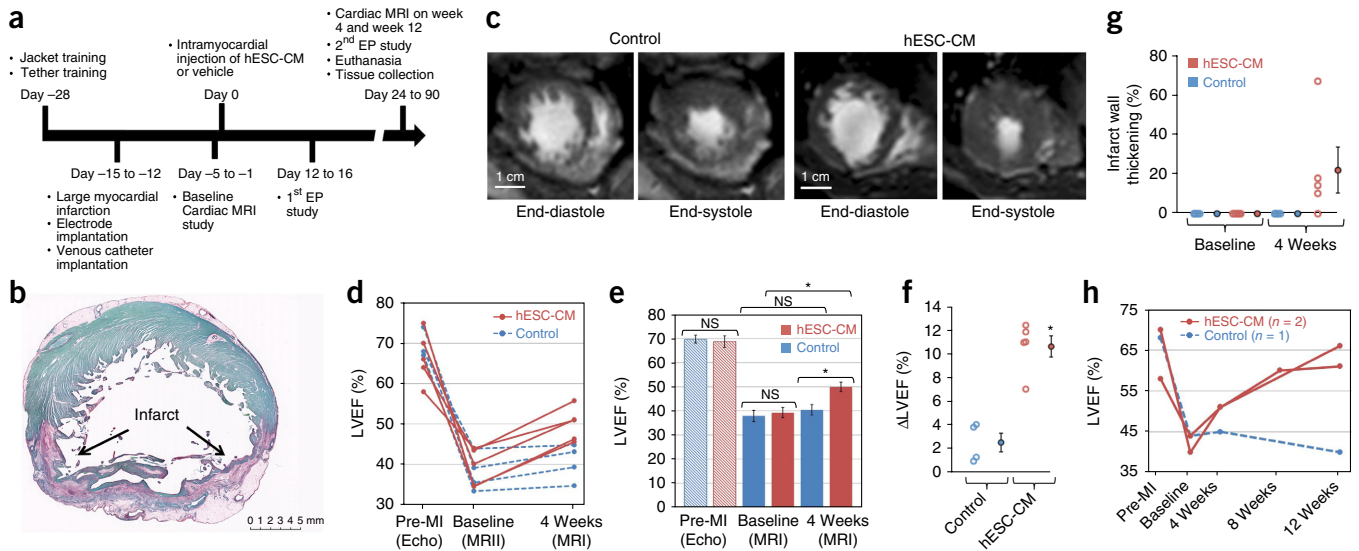
Over the last 20 years, there have been extensive efforts to induce the heart to heal by muscle regeneration rather than scarring[7–9]. Progress is being made on multiple fronts, including inducing cardiomyocyte proliferation[10–15] and reprogramming fibroblasts into cardiomyocytes[16–18]. Here we focus on transplantation of human cardiomyocytes derived from hESCs. These early-stage cardiomyocytes survive after transplantation and form new, maturing myocardium in animal models of myocardial infarction[19,20]. They improve cardiac function when transplanted into the mouse[21], rat[22,23], and guinea pig[24] infarct. A recent study from our group showed that hESC-CMs could remuscularize the infarcted hearts of macaque monkeys, where they formed electromechanical junctions with the host heart and beat in synchrony[25]. Although small-animal studies showed no evidence for arrhythmias, in monkeys hESC-CMs caused a transient period of ventricular arrhythmias[25]. Similar ventricular arrhythmias were reported when monkey pluripotent stem cell–derived cardiomyocytes were transplanted into infarcted monkey hearts[26].

The current study aimed to address two principal gaps in knowledge. The first was to learn whether hESC-CMs could restore

[1]Institute for Stem Cell and Regenerative Medicine, University of Washington, Seattle, Washington, USA. [2]Center for Cardiovascular Biology, University of Washington, Seattle, Washington, USA. [3]Division of Cardiology, Department of Internal Medicine, National Cheng Kung University Hospital, College of Medicine, National Cheng Kung University, Tainan, Taiwan. [4]Department of Medicine/Cardiology, University of Washington, Seattle, Washington, USA. [5]Department of Pathology, University of Washington, Seattle, Washington, USA. [6]City of Hope, Beckman Research Institute, Duarte, California, USA. [7]Washington National Primate Research Center, University of Washington, Seattle, Washington, USA. [8]Department of Pediatrics, University of Washington, Seattle Children's Hospital, Seattle, Washington, USA. [9]Department of Radiology, University of Washington, Seattle, Washington, USA. [10]Research Institute of Biology and Biophysics, National Research Tomsk State University, Tomsk, Russia. [11]Department of Bioengineering, University of Washington, Seattle, Washington, USA. [12]Present addresses: Division of Cardiology, Department of Internal Medicine, National Cheng Kung University Hospital, College of Medicine, National Cheng Kung University, Tainan, Taiwan (Y.-W.L.); Orbsen Therapeutics, LTD, Orbsen Buildings, National University of Ireland Galway, Galway, Ireland (L.C.); Uptake Medical Technologies, Seattle, Washington, USA. (S.A.T.). [13]These authors contributed equally to this work. Correspondence should be addressed to C.E.M. (murry@uw.edu).

Received 25 October 2017; accepted 6 May 2018; published online 2 July 2018; corrected after print 18 July 2018; doi:10.1038/nbt.4162

Figure 1 Effects of hESC-CM transplantation on cardiac function. (**a**) Timeline for the efficacy study in which non-human primates received 180 min ischemia and/or reperfusion in the mid-LAD vascular bed. Cardiac MRI is incorporated to measure cardiac dimensions and function. Electrophysiology studies are also included in the protocol to study the cause, inducibility, and severity of the ventricular arrhythmias. (**b**) A representative stain of a short-axis cross section of an infarcted non-human primate control heart with picrosirius red and fast green, where the infarct collagen is red and healthy myocardium is green. The infarct is transmural, with sparing of subendocardial myocardium. These experiments were repeated four times for controls and five times for hESC-CM treatment, with similar results. Scale bar, 5 mm. (**c**) Representative short-axis cine MRI at end-diastolic and end-systolic phases of the cardiac cycle at 4 weeks after treatment (6 weeks after MI). Blood in the chamber appears bright. There is greater ejection of blood in the hESC-CM heart during systole. These experiments were repeated four times for controls and five times for hESC-CM treatment, with similar results. Scale bar, 1 cm. (**d**) Plot of LVEF for individual subjects (four control animals, blue; five hESC-CM-treated animals, red) before infarction (pre-MI), at the post-infarction baseline (1 d before injection) and at 1 month after treatment. All hESC-CM hearts show significant improvement, while there is minimal improvement in controls. (**e**) Mean LVEF is comparable between groups before infarction and at post-infarction baseline ($P > 0.05$, paired t-test, df = 4) but shows a considerable improvement after hESC-CM treatment (*$P = 0.004$, paired t-test, df = 4). Data are from four biologically independent control animals and five hESC-CM-treated animals. Error bars, mean ± s.e.m. Individual data points are shown in 1 d. NS, not significant. (**f**) Change in LVEF (ΔLVEF) from baseline to 4 weeks is significantly greater in hESC-CM hearts than in controls. Data are from four biologically independent control animals and five hESC-CM-treated animals. Error bars, mean ± s.e.m. (*$P = 0.004$, two-tailed t-test, df = 7). (**g**) There is a variable trend ($P = 0.135$, paired t-test, df = 7) toward increased systolic thickening of the infarcted wall in hESC-CM-treated animals. Data are from four biologically independent control animals and five hESC-CM-treated animals. Error bars, mean ± s.e.m. (**h**) Extending survival to 12 weeks demonstrates a modest reduction in LVEF in control hearts and further improvement with hESC-CM treatment. This indicates the benefits seen at 4 weeks are stable with the potential for substantial further improvement.

contractile function in physiologically relevant large animals. For this we chose the non-human primate *Macaca nemestrina* because of its evolutionary proximity to humans, the similarity of the two species' cardiovascular systems, and because it is a well-established model in transplantation biology. This model should yield the best possible prediction of the human response to hESC-CM transplantation. The second was to understand the physiological basis for the ventricular arrhythmias induced by hESC-CMs. We report here that hESC-CMs provide robust and durable improvement in cardiac function in the infarcted macaque heart. We also provide evidence that graft-induced arrhythmias result from pacemaker-like activity rather than abnormal conduction.

RESULTS

hESC-CMs improve ventricular function

The central hypothesis of this study was that hESC-CM would remuscularize the hearts of macaque monkeys and restore their function after myocardial infarction. To assess the impact of hESC-CM transplantation on left ventricular structure and function, we developed techniques for cardiac magnetic resonance imaging (MRI) in the macaque. MRI is currently the gold standard for non-invasive imaging of cardiac structure, function, and tissue characterization. It provides reproducible measurements of left ventricular end-diastolic and end-systolic volumes, cardiac output, left ventricular ejection

fraction (LVEF), regional wall thickening during systole and infarct size[27,28]. Our previous study in macaques[25] created infarcts by occluding the distal left anterior descending (LAD) coronary artery for 90 min, followed by reperfusion. Pilot studies showed that this protocol gave a minimal reduction in ejection fraction, from ~65% at baseline to ~60% after infarction. For the functional studies here, we induced larger infarcts by occluding the mid-LAD for 3 h, followed by reperfusion (**Fig. 1a**). This induced transmural infarcts (**Fig. 1b** and **Supplementary Table 1**) and reduced ejection fraction to ~40% 2 weeks after infarction (**Fig. 1d,e**), creating a greater window for detecting functional improvement.

With this new infarction protocol in place, we undertook an efficacy study. Electrodes for electrocardiogram (EKG) telemetry were implanted at the time of infarction to assess spontaneous arrhythmias. Immunosuppressive agents were administered starting 5 d before cell delivery (**Fig. 1a**). Cells were administered ~14 d post-infarction by direct injection under surgical visualization. Cardiomyocytes were derived from the RUES2 hESC line in monolayer cultures using activin A and BMP4 to induce differentiation[22,24,25], or from the H7 hESC line in suspension cultures using small-molecule Wnt pathway modulation to induce differentiation[29]. The five animals studied by MRI received cardiomyocytes derived from the H7 hESC line. Purity of the cultures averaged 86–99% cardiomyocytes, based on flow cytometry for cardiac troponin T (**Supplementary Fig. 1**). We delivered

~750 million hESC-CMs or vehicle (RPMI media/pro-survival cocktail (PSC)) by surgically exposing the heart and injecting the cells intramuscularly into the infarct region and the border zones. MRI was performed 1 d before cell delivery and ~27 d after cell delivery, with all scans independently evaluated by three blinded observers. A subset of the animals underwent catheter-based electrophysiological studies at approximately day 14. Most macaques were euthanized ~28 d after cell transplantation, with the exception of two hESC-CM-treated and one control animal, which were given prolonged immunosuppression and studied by MRI at 12 weeks post-injection to assess the durability of the functional effects.

Seventeen macaques were initially enrolled in this study without randomization, and another two were enrolled for targeted mechanistic studies, described below. Eight animals were excluded from final MRI analysis due to protocol design or complications outlined in **Supplementary Figure 2**, only one of which was related to cell treatment, but nine successfully completed the infarction, cell, or vehicle injection, and multiple MRI scans (**Fig. 1c**). MRI scans were read by two blinded observers, with low interobserver variability (**Supplementary Fig. 3a**).

Prior to infarction, LVEF was 69.8 ± 1.3% in the control group and 68.8 ± 2.1% in the hESC-CM group (**Fig. 1d,e**; $P > 0.4$, NS). After infarction but before treatment, both groups exhibited similarly depressed LVEF, averaging 38.0 ± 2.3% in control animals and 39.4 ± 2.1% in hESC-CM-treated animals ($P > 0.67$, NS). At 4 weeks post-treatment, transplantation of hESC-CMs significantly improved LVEF (hESC-CM vs. control: 50.0 ± 1.9 vs. 40.5 ± 2.2%, $P < 0.05$; **Fig. 1d,e**). The effects of hESC-CM transplantation also could be seen by comparing the change in LVEF between day −1 and day 27: the control group showed an improvement of 2.5 ± 0.8%, whereas the hESC-CM-treated group improved by 10.6 ± 0.9% ($P = 0.001$; **Fig. 1f**). To assess contractile function in the infarct zone, we measured systolic wall thickening. Prior to therapy, all animals had 0% systolic LV wall thickening in the infarct zone, and all control hearts had 0% systolic LV wall thickening at 4 weeks. In contrast, after hESC-CM transplantation, wall thickening in the infarct improved to 22.0 ± 12% of the LV wall (**Fig. 1g**). However, because the improvement ranged from 0–67%, this was not statistically significant. Wall thickening in the non-infarcted region was not different between these two groups at any time (**Supplementary Fig. 4**), and there was no significant effect of cardiomyocyte transplantation on left ventricular end-diastolic volume. Taken together, these data indicate that formation of human myocardium in the infarcted non-human primate heart improves LV systolic function.

To test for the durability of the functional benefit, we studied three macaques at 3 months post-engraftment (two treated, one control; **Fig. 1h**). In the control animal, the LVEF decreased from 43.9% at day 27 to 40.4% at 3 months. In the hESC-CM-treated animals, LVEF improved from 51.1% and 51.0% at day 27 to 66.0% and 61.0% at 3 months. Thus, the benefit from hESC-CM therapy appears to be durable for 3 months, with function improving between 1 and 3 months.

Ventricular arrhythmia analysis

To study spontaneous arrhythmias, we outfitted macaques that had received 3-h coronary occlusion followed by reperfusion with EKG telemetry systems. Cardiac rhythms were recorded continuously for 24-h periods at 3-d intervals, and episodes of sustained ventricular tachycardia or accelerated idioventricular rhythm were quantified by one observer and validated by a second (**Supplementary Fig. 3b** and **Fig. 2a–d**). A total of six hESC-CM-treated and four control animals successfully completed this phase of the study. Arrhythmias

were quantified in hours/day and are shown for each animal in **Figure 2e,f**. Compared to our previous study using the small infarct model with amiodarone anti-arrhythmic treatment[25], there were two notable differences. First, both groups showed significantly ($P = 0.004$) more arrhythmias before cell and/or vehicle injection. This could be due either to the larger infarcts or the omission of the amiodarone from the current study. Second, unlike the small infarct model, where cell-treated animals had more frequent arrhythmias than controls, there was no statistical difference in the number or duration of arrhythmias between the two groups either before or after injection.

The telemetry data were highly variable, however, and one macaque deserves individual mention. This cell-treated animal developed extensive ventricular arrhythmias, including both ventricular tachycardia and accelerated idioventricular rhythm (AIVR). The ventricular arrhythmias began 10 d after cell injection and largely consisted of continuous (>20 h/day), monomorphic, wide complex tachycardia and AIVR (**Fig. 2f**, arrow). Although the animal was not in acute distress at any time, these arrhythmias were of sufficient severity that adequate MRI scans for functional studies were unattainable due to the high rate and irregularity. An arrhythmia of this duration was not observed in the control group. Despite the lack of statistical proof, we think that the most prudent interpretation is that one of the six cell-treated animals developed arrhythmias that likely were due to the hESC-CM graft.

The lower burden of engraftment arrhythmia in the current study could result from differences in the infarct model (large infarcts here), the cells (transgenic cells expressing the Ca^{2+} indicator GCaMP3 were used previously), or from unanticipated effects of the anti-arrhythmic drug, amiodarone[30], used previously. We therefore returned to the small infarct model and transplanted transgene-free cardiomyocytes and omitted amiodarone ($N = 1$ each; **Supplementary Fig. 5**). The transgene-free and amiodarone-free animals experienced a high burden of ventricular arrhythmias, providing evidence that the lower burden of arrhythmias in this study resulted from the larger infarcts.

To further characterize the ventricular arrhythmias and to assess arrhythmia vulnerability, we performed catheter-based electrophysiology studies using the CARTO III mapping system. Electrophysiology studies included programmed ventricular stimulation to induce arrhythmias, as well as activation and voltage mapping to characterize induced and spontaneous ventricular arrhythmias. We employed a standard, programmed, ventricular-stimulation protocol, where a series of entrainment stimuli were followed by up to three extra stimuli, delivered in succession at coupling intervals down to the ventricular refractory period, with or without isoproterenol infusion. Arrhythmia inducibility and severity were graded as previously reported[31]. The proposed mechanism of the tachycardia was determined by electrophysiological features including cycle length stability, pacing inducibility, and susceptibility to pace or electrical cardioversion. In instances where there was spontaneous initiation, significant cycle length variation without change in ventricular tachycardia morphology, and the inability to pace-induce or terminate with pacing or electrical cardioversion, the mechanism was presumed to be enhanced automaticity. In contrast, a relatively fixed cycle length and the ability to pace-induce, and susceptibility to pace or electrical cardioversion suggested a reentry mechanism.

Twelve electrophysiology studies were performed on eight animals (three control and five hESC-CM treated; one of the hESC-CM animals was from the small infarct protocol; **Supplementary Fig. 2**). Ten studies on eight animals yielded data on arrhythmia inducibility. In four of these (three hESC-CM treated, one control), ventricular stimulation resulted in induction of only brief episodes of non-sustained
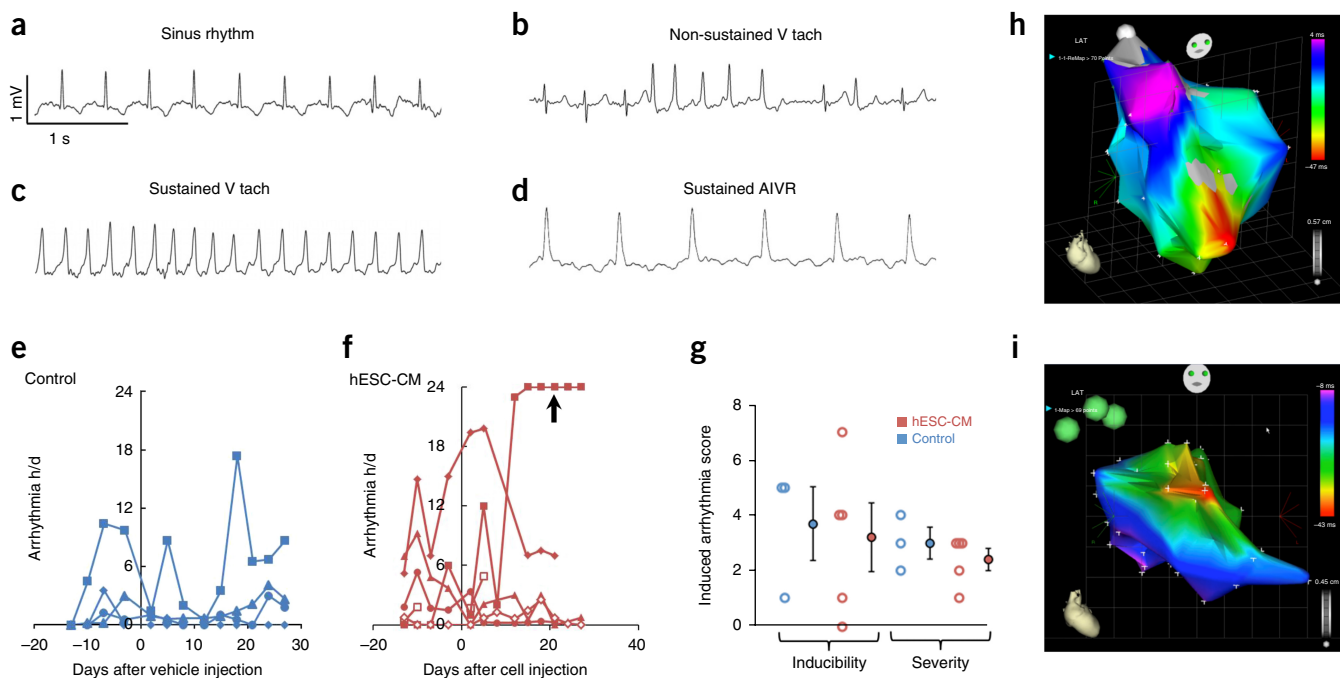
Figure 2 Analysis of arrhythmias. (**a–d**) Electrocardiograms from telemetry analysis of four biologically independent control animals and five hESC-CM-treated animals, demonstrating normal sinus rhythm (**a**), non-sustained ventricular tachycardia (**b**), sustained ventricular tachycardia (**c**), and sustained accelerated idioventricular rhythm (**d**). (**e,f**) Spontaneous ventricular arrhythmias in large infarct protocol (3-h mid-LAD occlusion) for four biologically independent control animals (**e**) and five biologically independent hESC-CM-treated animals (**f**) were recorded as h/d (24 h). Both groups have ventricular arrhythmias before and after injection (day 0), but the hESC-CM group had one subject with protracted arrhythmias (arrow), that likely are treatment-related. (**g**) Programmed electrical stimulation studies demonstrate that the inducibility and severity between biologically independent control ($N = 3$) and hESC-CM-treated hearts ($N = 5$) were not significantly different ($P = 0.816$, two-tailed t-test, df = 6 for inducibility; $P = 0.411$, two-tailed t-test, df = 6 for severity). Group data indicate mean ± s.e.m. (**h,i**) Electrical activation maps acquired using an endocardial catheter electrode. Red, early activation; magenta, late activation. (**h**) Activation in a non-infarcted macaque heart initiates at the apex (red; pointing toward the observer) and spreads toward the base. $N = 1$. (**i**) Activation map from an hESC-CM-engrafted heart during spontaneous ventricular tachycardia, with apex pointing toward lower right. Activation originates from an apparent point source in the anterior septum. No rotor was identified. This experiment was independently repeated twice with similar results.

ventricular tachycardia and were thus unable to be mapped. In two electrophysiology studies (one control and one hESC-CM-treated), we induced ventricular tachycardia that caused considerable hypotension, which precluded activation mapping and required termination of the arrhythmia with DC cardioversion. Quantitatively, there was no significant difference in arrhythmia inducibility between the vehicle-injected and hESC-CM-injected hearts (**Fig. 2g**). Similarly, the severity of the induced arrhythmias did not differ between the hESC-CM-treated and control animals (**Fig. 2g**). Thus, intramyocardial injection of hESC-CMs did not increase the risk and the severity of inducible ventricular arrhythmias.

Activation maps of ventricular tachycardia were obtained in two hESC-CM-treated and one control animal (**Fig. 2h,i**). In all cases, the ventricular tachycardia originated from a focal region. The control animal was studied twice, at 2 and 4 weeks post-injection, and in both studies the VT was induced, not spontaneous. In both studies the VT origin mapped to the low-voltage scar zone. The VT in the control heart was induced by pacing and could be terminated by overdrive pacing, both of which point to micro-reentry as the mechanism. Both cell-treated animals had spontaneous ventricular tachycardia when arrhythmia mapping began. These hearts could readily be overdrive-paced to 300 beats/min, but upon cessation of pacing, they returned almost immediately to their baseline tachycardic rates. We attempted to correct the arrhythmias with electrical cardioversion, but in both

instances, after a brief pause the rhythm resumed at its previous rapid rate. Taken together, these data suggest the arrhythmias in control hearts arise from a small focus of reentry, whereas those in the hESC-CM have features of abnormal impulse generation.

Tumor survey and structural analysis

One potential complication of hESC-CM therapy is teratoma formation or ectopic tissue growth[32]. All animals underwent a full necropsy by an experienced primate pathologist with a detailed gross and microscopic examination of the brain and all thoracic and abdominal organs. One cell-treated monkey had a microscopic focus of carcinoma in one kidney that was contained within small lymphatic and venous channels (**Supplementary Fig. 6a,b**). To test whether this tumor was of human or macaque origin, we performed *in situ* hybridization for human pan-centromeric genomic DNA sequences, and we also extracted DNA from the paraffin section for PCR genotyping. The tumor did not hybridize with the human-specific probe, and PCR detected only macaque DNA and was negative for human DNA (**Supplementary Fig. 6c–f**). This indicates that the tumor was of macaque origin. By immunohistochemistry, the tumor was negative for thyroid transcription factor-1 and GATA3. Conversely, it showed uniform, strong nuclear staining for Pax8. This immunophenotype is most consistent with a renal cell carcinoma[33]. No teratomas were detected in any animal, and no other atypical cellular masses were identified.
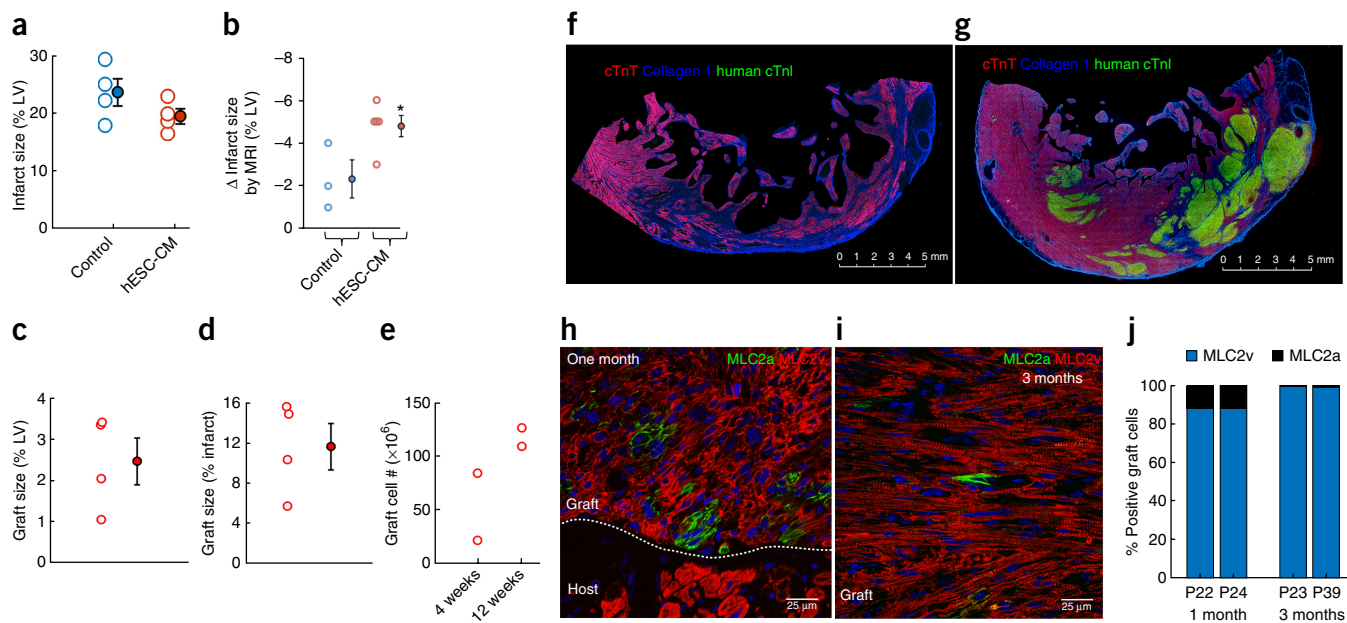
Figure 3 Structural assessment of infarct, graft size, and graft composition. (**a**) Histological infarct size was not different between groups at the end of the study. Each point is one heart. Data are from four biologically independent control animals and five hESC-CM-treated animals. Group data are means ± s.e.m. (**b**) Scar shrinkage by MRI from baseline to 4 weeks was significantly ($P < 0.05$, paired t-test) greater in hESC-CM hearts. Group data are means ± s.e.m. (**c**,**d**) Histological graft size expressed as a percentage of left ventricle and of the infarct. Data are from four biologically independent hESC-CM-treated animals. Group data are means ± s.e.m. (**e**) Graft cell number determined by histomorphometry. Note the increase in cell number from 4 to 12 weeks. Each point represents one heart, with two biologically independent replicates at each of 4 and 12 weeks. (**f**,**g**) Low magnification immunofluorescent images stained for cardiac troponin T (cTnT; red; human + monkey myocardium), human-specific cardiac troponin I (human cTnI; green; human myocardium) and type I collagen to identify scar tissue (blue). (**f**) Control heart showing transmural infarct and lateral border zone. Note the viable rim of host subendocardial myocardium and the thinned infarct wall compared to the border zone. This experiment was repeated in four biologically independent control animals with similar results. Scale bar, 5 mm. (**g**) hESC-CM engrafted heart showing large islands of human myocardium (green) within the infarct and lateral border zone. Note the relative preservation of wall thickness in the infarct region. This experiment was repeated in five biologically independent hESC-CM-treated hearts, with similar results in four. In one animal the graft was lost after 4 weeks due to interruption of immunosuppression. Scale bar, 5 mm. (**h**,**i**) Graft staining for definitive ventricular phenotype (MLC2v, red) or immature ventricular/atrial/nodal cardiomyocyte phenotype (MLC2a, green). (**h**) At 1 month post-engraftment, the majority of graft cells express MLC2v, but MLC2a+ cells are readily identified. Note that host cardiomyocytes express only MLC2v. This experiment was repeated in two biologically independent hESC-CM-treated hearts, with similar results. Scale bar, 25 μm. (**i**) At 3 months post-engraftment the graft comprised almost entirely definitive ventricular cardiomyocytes, and only rare MLC2a+ cells can be identified. This experiment was repeated in two biologically independent hESC-CM-treated hearts, with similar results. Scale bar, 25 μm. (**j**) Quantitation of MLC2v and MLC2a staining. At 3 months both grafts are 99% MLC2v+. Each bar represents one animal.

Histological analyses showed that infarcts in the sham-injected hearts averaged 23.6 ± 2.0% of the LV mass, whereas 19.9 ± 1.1% of the LV was infarcted in hESC-CM-treated hearts (**Fig. 3a**; $P = 0.18$, NS). We were able to obtain paired measurements of infarct size in three control and five hESC-CM-treated hearts at baseline and at 4 weeks post-engraftment using delayed gadolinium-enhanced MRI (**Fig. 3b** and **Supplementary Fig. 7**). This showed greater scar shrinkage in the hESC-CM-engrafted infarcts (5.3 ± 0.2% vs. 2.3 ± 0.9% of the LV; $P < 0.05$). This implies that the original infarct size was 25.9% of the LV in controls and 25.2% of the LV in hESC-CM-treated hearts.

To specifically label wild-type hESC-CMs in the graft, we identified two monoclonal antibodies to human grafts in the primate heart. The cardiac troponin I (cTnI) antibody is human-specific, and the slow-skeletal troponin I (ssTnI) antibody recognizes the relatively immature human cells that still express this developmentally regulated isoform[34]. In archival hearts that had received GFP-expressing cardiomyocytes, these troponin antibodies labeled regions identical to those identified by immunostaining for GFP or via *in situ* hybridization for human pan-centromeric sequences (**Supplementary Fig. 8**). There was virtually no staining of macaque cardiomyocytes with either antibody. One macaque damaged its intravenous

catheter, resulting in interruption of immunosuppression at 5 weeks post-transplantation in a planned 3-month survival protocol. No graft was detected in this animal, presumably due to rejection, and it was excluded from graft size calculations. In all other animals, large grafts of human myocardium were readily identified. Grafts ranged from 5.7–15.6% of the infarct (11.6 ± 2.3%; **Fig. 3d**) and 1.1–3.4% of the LV (2.2 ± 0.7%; **Fig. 3c**). In control hearts the infarct was a transmural scar, with subendocardial sparing of the host myocardium and considerable wall thinning (**Fig. 3f**). In hESC-CM hearts, large grafts were readily identified, often measuring more than a centimeter in greatest dimension (**Fig. 3g**). Grafts were located in the central infarct region and in the border zone myocardium, suggesting little migration occurred from the original injection sites (**Supplementary Fig. 9**). We estimated the number of cardiomyocytes in the grafts using histomorphometry (**Fig. 3e**). At 4 weeks post-injection there were 21.7 and 83.9 million cardiomyocytes in the grafts. At 3 months there were 109 and 126 million cardiomyocytes in the grafts, suggesting expansion due to proliferation.

At 4 weeks post-engraftment, 90% of graft cells were definitive ventricular cardiomyocytes (MLC2v+/MLC2a−; **Fig. 3h–j**), and 10% typed as either atrial, sinoatrial, or immature ventricular cardiomyocytes
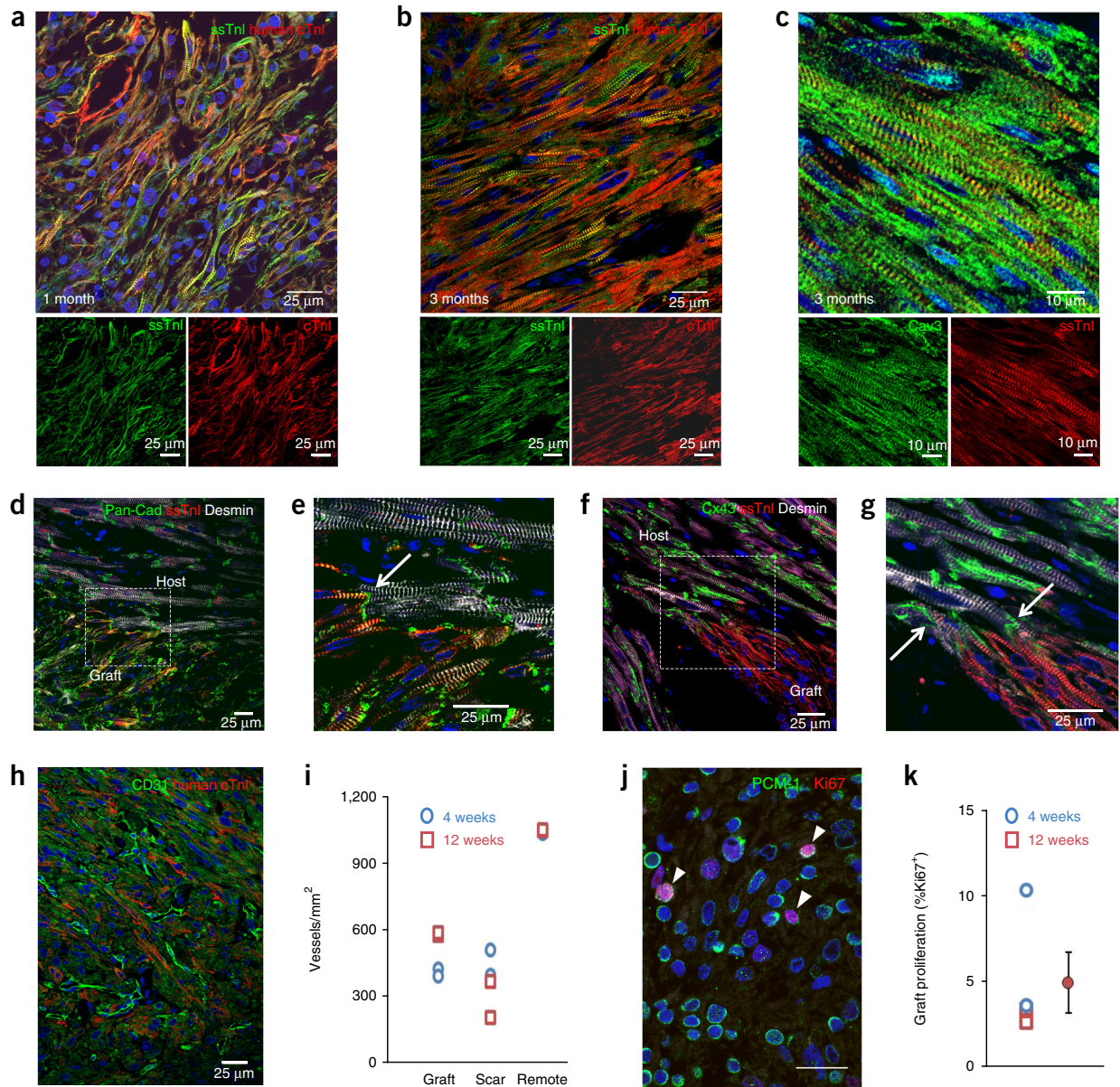
Figure 4 Graft maturation, integration, vascularization, and proliferation. (**a**,**b**) hESC-CM grafts stained for slow skeletal troponin I (ssTnI, green) and human cardiac troponin I (cTnI, red). Merged image on top, individual channels below. Scale bar, 25 μm. (**a**) At 1 month the hESC-CMs are relatively small, have peripheral myofibrils and exhibit low cellular alignment. Low level expression of cTnI is evident. This experiment was repeated in two biologically independent hESC-CM-treated hearts with similar results. (**b**) At 3 months the cells have hypertrophied, have myofibrils throughout the cytoplasm, and are better aligned. Increased expression of cTnI is evident. This experiment was repeated in two biologically independent hESC-CM-treated hearts with similar results. (**c**) At 3 months, graft T-tubule networks are present, shown by caveolin-3 staining (Cav3, green). ssTnI, red. This experiment was repeated in two biologically independent hESC-CM-treated hearts with similar results. Scale bar, 10 μm. (**d**) Interface of 3-month graft and host myocardium stained for pan-cadherin (green), ssTnI (human graft, red), and desmin (graft + host, white). This experiment was repeated in two biologically independent hESC-CM-treated hearts with similar results. Scale bar, 25 μm. (**e**) Magnified image of region boxed in **d** demonstrates cadherin-positive adherens junction at intercalated disk between graft and host (arrow). This experiment was repeated in two biologically independent hESC-CM-treated hearts with similar results. Scale bar, 25 μm. (**f**) Interface of 3-month graft and host myocardium stained for connexin43 (Cx43, green), ssTnI (human graft, red) and desmin (graft + host, white). This experiment was repeated in two biologically independent hESC-CM-treated hearts with similar results. Scale bar, 25 μm. (**g**) Magnified image of region boxed in **f** demonstrates connexin43-positive gap junctions at intercalated disks between graft and host (arrows). This experiment was repeated in two biologically independent hESC-CM-treated hearts with similar results. Scale bar, 25 μm. (**h**) Vascularization of the human myocardium (human cTnI-positive, red) by host microvessels is demonstrated by staining endothelial cells for CD31 (green). This experiment was repeated in four biologically independent hESC-CM-treated hearts with similar results. Scale bar, 25 μm. (**i**) Quantitation of vascular density in graft, scar, and remote myocardium at 4 and 12 weeks. Each point is one heart. Data are from four biologically independent control animals and four hESC-CM-treated animals. (**j**) Proliferation of 4-week hESC-CM graft demonstrated by staining for pericentriolar material-1 (PCM-1; green) and Ki67 (red). Cardiomyocyte nuclei in cell cycle are indicated by arrowheads. This experiment was repeated in four biologically independent hESC-CM-treated hearts with similar results. Scale bar, 20 μm. (**k**) Quantitation of graft cardiomyocyte proliferation at 4 weeks and 12 weeks. Each point is one heart. Data are from two biologically independent hESC-CM-treated hearts each at 2 and 4 weeks. Group data are mean ± s.e.m. for all four hearts.

(MLC2a$^+$/MLC2v$^-$); only rare double-positive cells were identified. By 3 months post-transplantation, 99% of graft cells were MLC2v$^+$, with <1% still expressing MLC2a. This indicates that the vast majority of cardiomyocytes generated by the differentiation protocol used in this study adopted a ventricular phenotype after transplantation, although expression of MLC2v is time-dependent.

Cardiomyocyte grafts showed considerable maturation *in vivo*. At 4 weeks post-transplantation (**Fig. 4a**) the cardiomyocytes were relatively small, had myofibrils principally at the cell periphery, and their alignment was disheveled. Additionally, the junctional proteins N-cadherin and connexin43 were distributed circumferentially (**Supplementary Fig. 10**). At 3 months, the cardiomyocytes were larger, had myofibrils throughout the cytoplasm, and were better aligned (**Fig. 4b**). N-cadherin was often polarized to intercalated disk-like structures, whereas connexin43 remained distributed circumferentially, though to a lesser extent than at 4 weeks (**Supplementary Fig. 10**). Additionally, by 3 months the hESC-CMs had readily discernible caveolin 3$^+$ invaginations of the sarcolemma that likely represent T-tubule networks (**Fig. 4c**). Although relatively immature, the 4-week grafts already had begun switching from the fetal ssTnI to the adult cTnI isoforms (**Fig. 4a**). Increased intensity of cTnI staining was readily apparent at 3 months (**Fig. 4b**), again indicating maturation. Areas of electromechanical integration were readily identified in all hearts where hESC-CMs formed N-cadherin$^+$ adherens junctions and connexin43$^+$ gap junctions with host cardiomyocytes (**Fig. 4d–g**).

Grafts had an extensive network of CD31$^+$ blood vessels (**Fig. 4h,i**), indicating vascularization by the host coronary circulation. At 4 weeks, grafts averaged 406 ± 11 vessels/mm^2, and this increased to 576 ± 4 vessels/mm^2 at 3 months, likely reflecting ongoing angiogenesis. In contrast, the infarct scar around the graft showed a time-dependent decline in vascular density, from 450 ± 40 vessels/mm^2 at 4 weeks to 284 ± 58 vessels/mm^2 at 3 months. Vascular density in the remote myocardium did not change over time, averaging $1,034 \pm 1.2$ and $1,043 \pm 2.5$ vessels/mm^2 at 4 weeks and 3 months, respectively.

Graft cardiomyocyte proliferation was measured by double staining for pericentriolar material-1 (PCM-1) and Ki67. PCM-1 marks the outer perimeter of cardiomyocyte nuclei[35], and Ki67 is a pan-cell-cycle epitope. Graft cell proliferation was detected in all hearts (**Fig. 4j,k**). At 4 weeks, graft cardiomyocyte proliferation rates were 10.3% and 3.5%. At 12 weeks, the proliferation rates were 2.6% and 3.5%. This demonstrates that considerable cell cycle activity occurs in the grafted cardiomyocytes, and coupled with the measured increase in graft cell number between 4 and 12 weeks, suggests that these are complete cell divisions rather than increases in ploidy.

The large size of these grafts made visualization by cardiac MRI possible. Using delayed gadolinium enhancement, three animals showed the appearance of islands of new tissue (viable Gd-negative tissue) within the infarcted anterior wall and septum at 1 and 3 months after treatment (**Fig. 5a–c**). These islands were ~1 cm in maximal dimension. By carefully cross-registering histology and MRI scans, we identified regions of human myocardium, >1 cm in maximal dimension, that corresponded to these Gd-negative regions in the MRI images (**Fig. 5d,e**). Masses of this size are easily visualized by MRI, leading us to conclude that it is possible to image large-scale regeneration from hESC-CM grafts.

DISCUSSION

A long-term goal of our program is to remuscularize the heart after myocardial infarction, and thereby improve its function. We have shown here that hESC-CMs can remuscularize infarcts in macaque monkey hearts and, in so doing, reduce scar size and restore significant
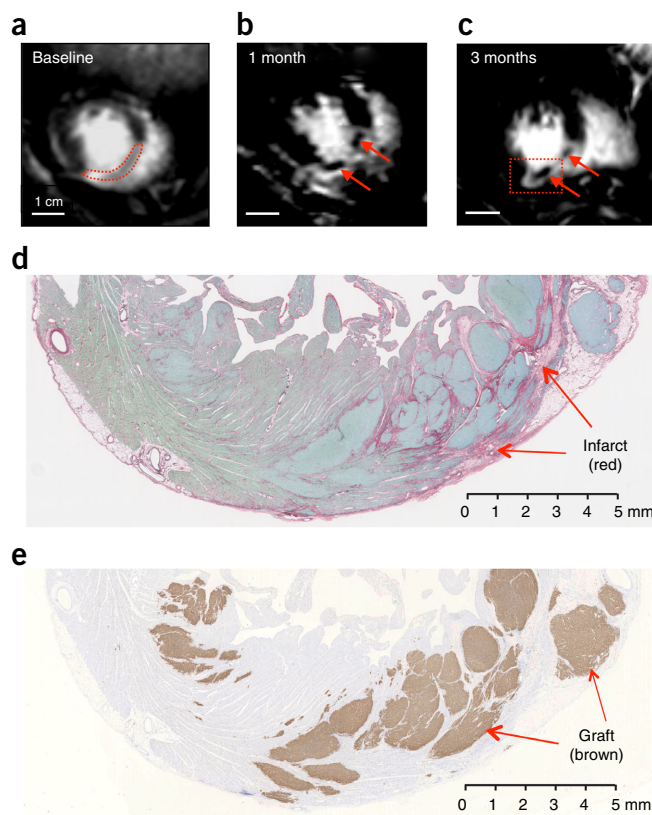

Figure 5 Visualization of grafts by MRI. (**a–c**) Delayed Gd enhanced MR images of macaque heart to identify the infarct scar. Blood in the chambers appears bright. Viable myocardium appears dark, and infarcted tissue appears light gray. The same short-axis region of the heart is shown in each scan. (**a**) At baseline, the infarct is a homogeneous tissue located in the anterior wall and interventricular septum (outlined by red dotted line). (**b,c**) At 1 month and 3 months post-engraftment, new areas of viable dark (Gd-negative) tissue appear within the infarct (arrows). (**d**) Histological section corresponding to the region boxed in **c**, stained with picrosirius red to identify collagen and fast green to identify myocardium. Infarct scar is readily identifiable as red tissue, but it contains islands of green tissue consistent with myocardium. Scale bar, 5 mm. (**e**) Adjacent section from region boxed in **c** stained for human cTnT (brown) to identify human myocardial graft. There is extensive human myocardium within the infarct and in the lateral border zone, measuring >1 cm in maximal dimension. Note that human myocardium within the scar would be visible by MRI, but grafts in the border zone host myocardium would be MRI-invisible, since both exclude Gd. This experiment was repeated four times with biologically independent hESC-CM-treated animals, with similar results found in three. In one animal, the graft could not reliably be distinguished by MRI.

levels of cardiac function. The infarcts studied were large, reducing ejection fraction from 69% to ~40%. No significant spontaneous recovery occurred in the vehicle-injected group (~2.5%), whereas all hESC-CM-treated hearts showed significant recovery at 4 weeks ($10.6 \pm 0.9\%$). Based on studies on three macaques extending to 3 months, the benefit to cardiac function appears durable, with further functional improvement between 1 and 3 months. Although pluripotent stem cell derivatives can cause teratomas[32,36,37], none were observed in the current study.

The 20% absolute improvement in LVEF seen in the two hESC-CM hearts studied at 3 months was striking and shows that substantial mechanical improvement can occur between 1 and 3 months.

Shiba *et al.*[26] also found significant improvement in LVEF after transplantation of allogeneic macaque induced pluripotent stem cell (iPSC)-derived cardiomyocytes into macaque infarcts[26]. The mechanical benefit could, in principle, result from direct mechanical force from the graft and/or paracrine signals[38] that enhance function of the host myocardium. We have shown that hESC-CM grafts form gap junctions with host myocardium and beat in synchrony in rat, guinea pig, and primate hearts[24,25,39]. The fact that grafts in the present study are large and beat in synchrony with host myocardium is consistent with a direct graft contribution to contractile function, as are the increased hypertrophy and maturation of engrafted cardiomyocytes. There also is evidence for paracrine effects of human pluripotent stem cell derivatives in the heart. Zhu *et al.*[40] recently reported that hESC-derived cardiac progenitors enhanced function of non-human primate hearts, even though the cells were rejected. That study differed from ours in many ways, including giving progenitors instead of definitive cardiomyocytes, using a dose that was ~1% of ours, delivering cells immediately after a permanent coronary occlusion instead of 2 weeks after ischemia reperfusion, and using an immunosuppression regimen that did not prevent rejection. Tachibana *et al.*[41] found that hESC- and hiPSC-derived cardiomyocytes could enhance function of the infarcted mouse heart with minimal engraftment, and they also attributed this benefit to paracrine signaling. These two papers demonstrate that human cardiac progenitors and cardiomyocytes can have benefits through indirect, paracrine mechanisms.

A major goal of this study was to understand the basis for ventricular arrhythmias associated with human cardiomyocyte engraftment. Mouse ESC-derived cardiomyocytes, grafted into the infarcted mouse heart, led to increased spontaneous arrhythmias[42,43], yet decreased susceptibility to pacing-induced arrhythmias[44]. When human ESC-CMs were transplanted into injured guinea pig hearts, our group found no effects on spontaneous arrhythmias and reduced susceptibility to pacing-induced arrhythmias[24]. In contrast, hESC-CMs transplanted into the hearts of macaque monkeys with small infarcts induced transient ventricular arrhythmias[25,45]. Similar arrhythmias were noted when allogeneic monkey iPSC-derived cardiomyocytes were transplanted into infarcted monkey hearts[26]. The similarity of arrhythmias in that allogeneic model and our xenogenic model suggests that species incompatibility is not the basis for arrhythmias in our model.

Although graft-induced arrhythmias appear to be less frequent in the large infarct model used here, at least one of our cell-treated macaques experienced ventricular arrhythmias that can reasonably be attributed to the graft. This raises the possibility that similar arrhythmias could occur in humans treated using the same protocol. We systematically ruled out effects from the GCaMP transgene and the amiodarone drug treatment used in our previous study. Although we hypothesized that hESC-CM grafts were creating tracts of slow conduction leading to reentrant arrhythmias, this was not supported by the data. In electrical mapping studies, no reentrant pathway could be identified; rather, the impulse appeared to originate from a point source in the graft region. This indicates either an ectopic activation source or a reentry pathway smaller than the resolution of our mapping (~1 cm). The arrhythmia could not be extinguished either by overdrive pacing or by electrical cardioversion, both of which favor ectopic impulse generation. Finally, there was no difference in susceptibility of the engrafted hearts versus the vehicle-injected hearts to arrhythmias induced by programmed electrical stimulation, which typically elicits reentrant arrhythmias in regions of abnormal conduction. All these characteristics point toward a disorder of impulse generation (either pacemaking or after depolarizations) rather than

reentry as the underlying cause for hESC-CM-induced arrhythmias. These insights may help identify pharmacological or cell-autonomous interventions to limit arrhythmias in the future.

There are several limitations to this study. First, because it is a primate study, group sizes are smaller than is typical for a small animal study. Although we demonstrate statistically robust data for mechanical improvement, some experiments showed trends that would require larger groups for statistical significance. This is mitigated in part by the high animal-to-animal consistency in physiological responses. Second, this xenotransplantation study does not address the human immune response to allogeneic cardiomyocytes. While testing human cardiomyocytes is essential for regulatory approval, allogeneic data from monkeys would be useful.

The functional recovery seen in the current study was larger than we have observed using rat[22] or guinea pig[24] models of myocardial infarction, even though grafts occupied a similar fraction of the ventricle. This finding is likely explained by the greater physiological match between human and macaque. The therapeutic effect may be further augmented when human cardiomyocytes are transplanted into diseased human hearts.

METHODS

Methods, including statements of data availability and any associated accession codes and references, are available in the online version of the paper.

Note: Any Supplementary Information and Source Data files are available in the online version of the paper.

AUTHOR CONTRIBUTIONS
Y.-W.L. designed experiments, conducted animal studies, analyzed data and edited the manuscript. B.C. designed experiments, conducted animal studies, performed histology studies, analyzed data and edited the manuscript. X.Y. performed histology, histomorphometry, analyzed data, prepared figures, and edited the manuscript. J.A.F. prepared cells for transplantation and edited the manuscript. F.A.K. prepared cells for transplantation and edited the manuscript. A.F.-T. prepared cells for transplantation and edited the manuscript. L.C. supervised cell manufacturing. K.W.V. designed experiments, conducted animal studies, and provided veterinary care. C.A.A. designed experiments and conducted animal studies. A.B. performed necropsies and provided pathology consultation. J.O. conducted animal studies and edited the manuscript. C.W.D. designed experiments, conducted animal studies and edited the manuscript. Z.L.S. conducted animal studies and edited the manuscript. S.P.S. designed experiments, conducted electrophysiology studies, analyzed data and edited the manuscript. S.A.T. conducted animal studies, analyzed data and edited the manuscript. H.T. conducted animal studies and edited the manuscript. A.V.N. performed MRI studies, analyzed data and edited the manuscript. S.K.D. performed histology. M.S.L. analyzed MRI scans. J.L. analyzed MRI scans and edited the manuscript. D.W.H. advised on and performed microscopy. H.R. designed experiments, performed histology, conducted molecular analyses, analyzed data, and prepared figures. L.P. designed experiments, analyzed data and edited the manuscript.

Reprints and permissions information is available online at http://www.nature.com/reprints/index.html. Publisher's note: Springer Nature remains neutral with regard to jurisdictional claims in published maps and institutional affiliations.

1. Forouzanfar, M.H. *et al.* Assessing the global burden of ischemic heart disease, part 2: analytic methods and estimates of the global epidemiology of ischemic heart disease in 2010. *Glob. Heart* **7**, 331–342 (2012).
2. Laflamme, M.A. & Murry, C.E. Heart regeneration. *Nature* **473**, 326–335 (2011).
3. Eschenhagen, T. *et al.* Cardiomyocyte regeneration: a consensus statement. *Circulation* **136**, 680–686 (2017).
4. Bergmann, O. *et al.* Evidence for cardiomyocyte renewal in humans. *Science* **324**, 98–102 (2009).
5. Soonpaa, M.H. & Field, L.J. Survey of studies examining mammalian cardiomyocyte DNA synthesis. *Circ. Res.* **83**, 15–26 (1998).
6. van Berlo, J.H. *et al.* c-kit+ cells minimally contribute cardiomyocytes to the heart. *Nature* **509**, 337–341 (2014).
7. Burridge, P.W., Sharma, A. & Wu, J.C. Genetic and epigenetic regulation of human cardiac reprogramming and differentiation in regenerative medicine. *Annu. Rev. Genet.* **49**, 461–484 (2015).
8. Gerbin, K.A. & Murry, C.E. The winding road to regenerating the human heart. *Cardiovasc. Pathol.* **24**, 133–140 (2015).
9. Lee, R.T. & Walsh, K. The future of cardiovascular regenerative medicine. *Circulation* **133**, 2618–2625 (2016).
10. Hassink, R.J. *et al.* Cardiomyocyte cell cycle activation improves cardiac function after myocardial infarction. *Cardiovasc. Res.* **78**, 18–25 (2008).
11. Xin, M. *et al.* Hippo pathway effector Yap promotes cardiac regeneration. *Proc. Natl. Acad. Sci. USA* **110**, 13839–13844 (2013).
12. Heallen, T. *et al.* Hippo signaling impedes adult heart regeneration. *Development* **140**, 4683–4690 (2013).
13. Heallen, T. *et al.* Hippo pathway inhibits Wnt signaling to restrain cardiomyocyte proliferation and heart size. *Science* **332**, 458–461 (2011).
14. Shapiro, S.D. *et al.* Cyclin A2 induces cardiac regeneration after myocardial infarction through cytokinesis of adult cardiomyocytes. *Sci. Transl. Med.* **6**, 224ra27 (2014).
15. Leach, J.P. *et al.* Hippo pathway deficiency reverses systolic heart failure after infarction. *Nature* **550**, 260–264 (2017).
16. Liu, Z. *et al.* Single-cell transcriptomics reconstructs fate conversion from fibroblast to cardiomyocyte. *Nature* **551**, 100–104 (2017).
17. Zhou, H. *et al.* ZNF281 enhances cardiac reprogramming by modulating cardiac and inflammatory gene expression. *Genes Dev.* **31**, 1770–1783 (2017).
18. Cao, N. *et al.* Conversion of human fibroblasts into functional cardiomyocytes by small molecules. *Science* **352**, 1216–1220 (2016).
19. Kadota, S., Pabon, L., Reinecke, H. & Murry, C.E. In vivo maturation of human induced pluripotent stem cell-derived cardiomyocytes in neonatal and adult rat hearts. *Stem Cell Reports* **8**, 278–289 (2017).
20. Cho, G.S. *et al.* Neonatal transplantation confers maturation of PSC-derived cardiomyocytes conducive to modeling cardiomyopathy. *Cell. Rep.* **18**, 571–582 (2017).
21. van Laake, L.W. *et al.* Human embryonic stem cell-derived cardiomyocytes survive and mature in the mouse heart and transiently improve function after myocardial infarction. *Stem Cell Res. (Amst.)* **1**, 9–24 (2007).
22. Laflamme, M.A. *et al.* Cardiomyocytes derived from human embryonic stem cells in pro-survival factors enhance function of infarcted rat hearts. *Nat. Biotechnol.* **25**, 1015–1024 (2007).
23. Caspi, O. *et al.* Transplantation of human embryonic stem cell-derived cardiomyocytes improves myocardial performance in infarcted rat hearts. *J. Am. Coll. Cardiol.* **50**, 1884–1893 (2007).
24. Shiba, Y. *et al.* Human ES-cell-derived cardiomyocytes electrically couple and suppress arrhythmias in injured hearts. *Nature* **489**, 322–325 (2012).
25. Chong, J.J. *et al.* Human embryonic-stem-cell-derived cardiomyocytes regenerate non-human primate hearts. *Nature* **510**, 273–277 (2014).
26. Shiba, Y. *et al.* Allogeneic transplantation of iPS cell-derived cardiomyocytes regenerates primate hearts. *Nature* **538**, 388–391 (2016).
27. Naumova, A.V., Modo, M., Moore, A., Murry, C.E. & Frank, J.A. Clinical imaging in regenerative medicine. *Nat. Biotechnol.* **32**, 804–818 (2014).
28. Zhang, W.Y., Ebert, A.D., Narula, J. & Wu, J.C. Imaging cardiac stem cell therapy: translations to human clinical studies. *J. Cardiovasc. Transl. Res.* **4**, 514–522 (2011).
29. Chen, V.C. *et al.* Development of a scalable suspension culture for cardiac differentiation from human pluripotent stem cells. *Stem Cell Res. (Amst.)* **15**, 365–375 (2015).
30. Hohnloser, S.H., Klingenheben, T. & Singh, B.N. Amiodarone-associated proarrhythmic effects. A review with special reference to torsade de pointes tachycardia. *Ann. Intern. Med.* **121**, 529–535 (1994).
31. Chelsky, L.B. *et al.* Caffeine and ventricular arrhythmias. An electrophysiological approach. *J. Am. Med. Assoc.* **264**, 2236–2240 (1990).
32. Nussbaum, J. *et al.* Transplantation of undifferentiated murine embryonic stem cells in the heart: teratoma formation and immune response. *FASEB J.* **21**, 1345–1357 (2007).
33. Kuroda, N., Tanaka, A., Ohe, C. & Nagashima, Y. Recent advances of immunohistochemistry for diagnosis of renal tumors. *Pathol. Int.* **63**, 381–390 (2013).
34. Bedada, F.B. *et al.* Acquisition of a quantitative, stoichiometrically conserved ratiometric marker of maturation status in stem cell-derived cardiac myocytes. *Stem Cell Reports* **3**, 594–605 (2014).
35. Bergmann, O. *et al.* Identification of cardiomyocyte nuclei and assessment of ploidy for the analysis of cell turnover. *Exp. Cell Res.* **317**, 188–194 (2011).
36. Swijnenburg, R.J. *et al.* Embryonic stem cell immunogenicity increases upon differentiation after transplantation into ischemic myocardium. *Circulation* **112** Suppl, I166–I172 (2005).
37. Lee, A.S., Tang, C., Rao, M.S., Weissman, I.L. & Wu, J.C. Tumorigenicity as a clinical hurdle for pluripotent stem cell therapies. *Nat. Med.* **19**, 998–1004 (2013).
38. Hodgkinson, C.P., Bareja, A., Gomez, J.A. & Dzau, V.J. Emerging concepts in paracrine mechanisms in regenerative cardiovascular medicine and biology. *Circ. Res.* **118**, 95–107 (2016).
39. Gerbin, K.A., Yang, X., Murry, C.E. & Coulombe, K.L. Enhanced electrical integration of engineered human myocardium via intramyocardial versus epicardial delivery in infarcted rat hearts. *PLoS One* **10**, e0131446 (2015).
40. Zhu, K. *et al.* Lack of remuscularization following transplantation of human embryonic stem cell-derived cardiovascular progenitor cells in infarcted nonhuman primates. *Circ. Res.* **122**, 958–969 (2018).
41. Tachibana, A. *et al.* Paracrine effects of the pluripotent stem cell-derived cardiac myocytes salvage the injured myocardium. *Circ. Res.* **121**, e22–e36 (2017).
42. Liao, S.Y. *et al.* Overexpression of Kir2.1 channel in embryonic stem cell-derived cardiomyocytes attenuates posttransplantation proarrhythmic risk in myocardial infarction. *Heart Rhythm* **10**, 273–282 (2013).
43. Liao, S.Y. *et al.* Proarrhythmic risk of embryonic stem cell-derived cardiomyocyte transplantation in infarcted myocardium. *Heart Rhythm* **7**, 1852–1859 (2010).
44. Roell, W. *et al.* Engraftment of connexin 43-expressing cells prevents post-infarct arrhythmia. *Nature* **450**, 819–824 (2007).
45. Chong, J.J. & Murry, C.E. Cardiac regeneration using pluripotent stem cells—progression to large animal models. *Stem Cell Res. (Amst.)* **13**, 654–665 (2014).

ONLINE METHODS

Animal care. General features of primate care following infarction and cell therapy (see also **Supplementary Notes**).

Post-infarct animals were monitored daily with particular attention paid to signs of distress, which may indicate post-procedure pain or symptoms of heart failure. If necessary, furosemide was injected to relieve limb edema or pulmonary congestion, manifest as increased respiratory rate and crackles on auscultation of the chest. Dobutamine infusion was started for clinical signs of poor end-organ perfusion in the setting of heart failure or cardiogenic shock. In the event of frequent PVCs or AIVR on telemetry, a short course of lidocaine infusion was given. For any hemodynamically unstable arrhythmias, the animals would undergo the normal algorithm of advanced cardiovascular life support.

Surgical wounds were carefully examined for signs of infection. In the event of possible infection, wound swabs were obtained and sent for microbiology with the commencement of empirical antibiotics in consultation with veterinary staff. If there were any severe complications noted in the animal, we consulted the veterinarian staffs and treated as clinically appropriate. If the clinical or attending veterinarian diagnosed an untreatable complication, the animal was euthanized. All animals had full necropsies performed by an experienced primate pathologist.

Cell preparation. These studies were approved by the University of Washington Stem Cell Research Oversight Committee. Two lines of hESCs were used in this study. RUES2 cells (obtained from Rockefeller University) were expanded in monolayers in mouse embryonic fibroblast-conditioned medium. Differentiation was performed by replating the cells in high-density monolayers, followed by sequential treatment with recombinant human activin A and BMP4, as previously described[22,24,25,46]. Prior to cryopreservation, RUES2-derived cardiomyocytes were heat-shocked and treated with a pro-survival cocktail to enhance their survival after transplantation[22,25,46]. H7 hESCs (obtained from WiCell) were cultured, expanded, and differentiated in suspension-culture format by collaborators at the Center for Applied Technology Development at the City of Hope in California[29]. Pluripotent H7 cultures were expanded in the commercially available media, StemPro hESC SFM. For cardiac differentiation, pluripotent aggregates were cultured in RPMI-1640 supplemented with B-27 (with or without insulin). Differentiation

is induced by treatment with the small molecules Chir99021 and IWP-4. On day 21 of differentiation, cardiomyocyte aggregates were dissociated by treatment with Liberase TH and TrypLE. Dissociated cardiomyocytes were cryopreserved in CryoStor CS10 supplemented with 10 µM Y-27632 with freezing performed in a controlled-rate liquid nitrogen freezer. Four lots of H7-cardiomyocytes were received by dry-ice shipment, and stored in LN2 before use. Two lots of cardiomyocytes were thawed and blended in approximately equal numbers to produce consistent cell treatments for each of the five treated animals completing the study. Per the City of Hope Product Summary, cryopreserved cells and thawed cells averaged 96% cTnT positive and 85% viable. Following shipment and additional storage time, thawed cells were shown to be 86% viable using an NC200/ Via1-cassette (Chemometec, Denmark) and 87% cTnT positive (human IgG anti-cardiac troponin clone REA400; Miltenyi, Germany).

Approximately 3 h before transplantation, cryopreserved cardiomyocytes were thawed in a 37 °C water bath (2 min ± 30 s). RPMI-1640 supplemented with B-27 and ≥200 Kunitz Units/mL DNase I was added to the cell suspension to dilute the cryopreservation media. Subsequent wash steps were done using RPMI-1640 basal media in progressively smaller volumes in order to concentrate the cell suspension.

Before the last centrifugation step, the cell pellet was resuspended in a 5-factor Pro-Survival Cocktail (PSC). PSC consists of RPMI-1640 basal media supplemented with: 10 µM ZVAD-FMK/Caspase Inhibitor (Calbiochem/ EMD-Millipore); 50 nM TAT-BH4 / BCL-XL (Calbiochem/EMD-Millipore); 200 nM Cyclosporine A (Sandimmune/Novartis); 5 0 µM Pinacidil (Sigma); and 100 ng/ml IGF-1 (Peprotech). Unlike many of our previous studies, no Matrigel was used to deliver the cells.

After resuspension in PSC, the cell suspension was centrifuged so that sufficient volume of PSC supernatant could be removed in order to achieve a target cell density for injection (~7.5×10^8 cells in ~1.5 mL PSC). The final volume of the cell suspension was determined by the results of a count sampled before the final centrifugation step. Note that our previous study counted cells before the freezing step. Because there is a 25% cell loss after the thaw, this dose of 750 million cells is comparable to our previously reported dose of 1 billion[25].

Animal models. All procedures complied with and were approved by the University of Washington Animal Care and Use Committee.

Table 1 Data for individual macaques in MRI study

Animal #	Sex	Age (years, months)	Weight, kg	Infarct size, histology (% of LV)	Graft size (% of infarct)	Graft cell number (millions)	Pre-infarction LVEF by echo (%)	Post-infarction baseline MRI LVEDV (ml)	LVESV (ml)	LVEF (%)	Infarcted LVTh (%)	Infarct size (% of LV)	MRI 4 weeks after treatment LVEDV (ml)	LVESV (ml)	LVEF (%)	Infarcted LVTh (%)	Infarct size (% of LV)
								Control									
P14	M	6, 10	12.6	29.2	NA	NA	68	18.0	10.2	43.9	0	19	20.7	11.4	44.8	0	18
P15	F	9, 7	11.7	22.2	NA	NA	74	19.0	11.6	39.1	0	NA	23.6	13.4	43.1	0	NA
P18	F	10, 9	11.4	18.1	NA	NA	67	16.1	10.7	33.4	0	15	18.3	11.9	34.7	0	13
P20	F	6, 0	10.6	25.0	NA	NA	70	15.5	10.0	35.5	0	17	13.0	7.9	39.3	0	13
Mean		8	11.6	23.6	**NA**	**NA**	69.8	17.2	10.6	38.0	0	17	18.9	11.2	40.5	0	15
s.e.m.		1	0.4	2.3	**NA**	**NA**	1.3	0.8	0.4	2.3	0	1	2.2	1.2	2.2	0	1
								hESC-CM									
P22	F	15, 7	7.0	18.7	5.7	23.0	75	13.2	8.6	34.5	0	31	12.3	6.6	46.3	14	26
P23	F	11, 6	10.7	23.0	14.8	133.6	70	16.1	9.6	40.1	0	15	13.3	6.5	51.1	67	10
P24	F	12, 2	9.5	19.9	10.3	88.9	66	15.2	9.9	34.7	0	25	16.1	8.8	45.6	0	20
P25	F	6, 7	5.2	16.6	ND	ND	64	11.7	6.6	43.5	0	17	13.8	6.1	55.8	10	11
P39	F	14, 6	9.2	21.5	15.6	115.6	58	13.7	7.6	44.0	0	16	11.2	5.5	51.0	18	13
Mean		11	8.6	19.9	11.6	90.3	66.6	14.0*	8.5*	39.4	0	21	13.3*	6.7**	50.0*	22	16
s.e.m.		2	0.9	1.1	2.3	21.0	2.9	0.8	0.6	2.1	0	3	0.8	0.6	1.9	12	3

All hESC-CMs for these studies were derived from the H7 line.
LVEDV, left ventricular end-diastolic; LVESV, left ventricular end end-systolic volumes; NA, not applicable or not available; ND, not detected: graft was rejected at 5 weeks post-engraftment due to damage to the intravenous catheter and interruption of immunosuppression. This animal was excluded from graft size calculations. Infarcted LVTh, infarcted left ventricular wall systolic thickening.
*$P < 0.05$, control vs. hESC-CM treated; **$P < 0.01$, control vs. hESC-CM treated.

Non-human primate catheterization and surgery. *Macaca nemestrina* monkeys of either sex, weighing 5.2–12.6 kg, were obtained from the Washington National Primate Center. Ages are specified in **Table 1**. Macaques first underwent a 2- to 4-week period of acclimation and training to wear a mesh jacket with an exteriorized line that attached to a tether system to prevent removal of intravenous (i.v.) catheter and EKG electrodes. For all major surgeries and procedures, macaques were sedated with ketamine and propofol, intubated, and ventilated using sevoflurane or isoflurane to maintain anesthesia. Buprenorphine SR was administered to provide perioperative and postoperative pain relief.

Before myocardial infarction creation, an i.v. lidocaine bolus of 1 mg/kg and an infusion of 20 μg/kg/min were used to prevent ventricular arrhythmias. Heparin was delivered i.v. to maintain activated clotting times (ACT) of 250–350 s to prevent thrombus formation. Femoral artery access was obtained via direct cutdown followed by puncture with a 5F Terumo Glidesheath. Under fluoroscopic guidance (OEC 9800 Plus, GE Medical Systems), a 5F Convey guiding catheter (a modified FL3, Boston Scientific) was used to engage the left main coronary artery. A coronary guide wire and angioplasty balloon (Apex 2 × 8 mm PTCA Dilatation Catheter, Boston Scientific) were passed into the mid-left anterior descending artery (LAD). The balloon was inflated until the artery was occluded (as demonstrated by angiography) and left inflated for 180 min. Myocardial ischemia was confirmed by ST-segment elevation on EKG.

For telemetric monitoring, tunneled subcutaneous EKG electrodes were implanted (two in the chest wall and one in the abdomen; lead II equivalent) and connected to wireless Vetcheck modules (Vmed Technology) through the jacket/tether system. Dual lumen venous catheters were implanted and tunneled to allow peripheral blood sampling and intravenous drug administration with minimal distress to the animals. Immune suppression was achieved with three drugs. Methylprednisolone was given i.v. 30 mg/kg on the day before hESC-CM delivery, followed by maintenance doses of 6 mg/kg for 2 d, and then 3 mg/kg thereafter until monkeys were euthanized. Cyclosporine A was given i.v. to maintain serum trough levels of 200–250 μg/L from 5 d before hESC-CM delivery until macaques were euthanized. Finally, Abatacept (CTLA4-Ig) 12.5 mg/kg was administered subcutaneously on the day before hESC-CM and every 2 weeks thereafter. Ceftazidime, cefazolin, vancomycin, gentamycin, fluconazole, and acyclovir were administered for prophylaxis of opportunistic infections.

On approximately day 14 after myocardial infarction, macaques were anaesthetized and underwent left-sided thoracotomy. The heart was exposed and a pericardial cradle created. The infarct region was directly visualized, and hESC-CMs were delivered from an epicardial approach into the infarct and peri-infarct region via 15 injections each of 100 μl volume. Needle tips were placed within a preformed mattress suture, and the suture was cinched around the needle to facilitate cell retention. Three injections were delivered via the same epicardial puncture, changing the trajectory of the needle for each. The needle was carefully withdrawn and the mattress suture ligated. For control macaques, an equal volume of PSC vehicle was injected in the same manner as for hESC-CM delivery. Three injections were placed in the peri-infarct border zone, and two were placed into the central ischemic region. LAD coronary occlusion infarcts both the anterior free wall and the anterior 2/3 of the interventricular septum. Although the free wall is readily accessed from an epicardial approach, the septal wall is not visible. We targeted cells to the septum by passing the needle under the LAD artery and inferring the septal wall's location from the curvature of the left ventricular free wall.

Animals were regularly monitored by laboratory and Primate Center staff. Euthanasia was induced under deep anesthesia by i.v. injection of saturated KCl. Control and cell-treatment groups were allocated in an unblinded and non-randomized manner.

Post-surgery care. Post-infarct animals were monitored daily with particular attention paid to signs of distress, which may indicate post-procedure pain or symptoms of heart failure. If necessary, furosemide was injected to relieve pulmonary congestion or limb edema. Signs of distress, such as increased respiratory rate and crackles on auscultation of the chest were used to assess signs of pulmonary congestion. Surgical wounds were carefully examined for signs of infection. In the event of possible infection, wound swabs were obtained and sent for microbiology with the commencement of empirical antibiotics in

consultation with veterinary staff. If there were any severe complications noted in the animal, we consulted the veterinarian staffs and treated as clinically appropriate. If the clinical or attending veterinarian diagnosed an untreatable complication (lower extremity ischemia, renal and liver failure, femoral artery dissection), the animal was euthanized. All animals had full necropsies performed by an experienced primate pathologist. Individual procedure notes for each animal are available in the **Supplementary Procedures**.

Cardiac MRI. Cardiac MRI was performed before cell injection (2 weeks after MI) and at 4 and 12 weeks post cell-injection. *In vivo* imaging studies were conducted on a 3-Tesla Achieva clinical scanner (Philips, Best, Netherlands). Depending on the animal size, two overlapped Flex-M and Flex-L coils (dual-element, approximately 15 and 20 cm diameter, respectively) or an 8-element knee coil was used. Pediatric EKG leads were used for gating of MRI acquisitions. EKG, respiration rate, and arterial oxygen saturation, and body temperature was monitored continuously.

The cardiac MRI protocol included cine imaging for assessment for the LV geometry, global LV contractile function, regional systolic LV wall thickening and delayed gadolinium-enhanced imaging for assessment of the infarct size. Cine images were acquired with an RF-spoiled turbo field echo (T_1-TFE) sequence that generated 25–30 cardiac phases for 10–12 short-axis slices spanning the left ventricle. Acquisition parameters included a repetition time (TR) 3.9 msec, echo time (TE) 1.9 msec, a 15° flip angle (FA), 4 mm slice thickness (no gap), field of view (FOV) 120 × 120 mm², 1 mm² voxel size, 6–8 signal averages, retrospective EKG gating without breath hold.

Animals subsequently received an intravenous bolus injection of gadolinium-based contrast agent ProHance (Bracco Diagnostics Inc., Princeton, NJ) 0.2 mmol/kg, followed by a saline flush. At approximately 8 min after injection, inversion time (TI)-scout images were acquired for determination of TI to null signal from non-infarcted myocardium. At 9 min post-injection of contrast agent, phase-sensitive inversion recovery (PSIR) multislice images were acquired at the LV short axis to visualize the infarct: TR/TE 7.3/3.5 msec, FA 25°, voxel size 1.3 mm², FOV 150 × 150 mm², slice thickness 4 mm without gap, four averages. This was repeated in the long axis plane. Inversion time ranged from 280–350 msec, adjusted by the operator based on TI-scout values. Signal intensity threshold to differentiate normal myocardium from scar was set as 'Full Width Half Max'.

All MRI scans were analyzed by three independent reviewers who were blinded as to treatment and timing of the evaluations. Inter-observer variability was good, with an intraclass correlation coefficient of the average LVEF measurements was 0.978 (95% confidence interval (CI): 0.951–0.990, $P < 0.001$; **Supplementary Fig. 3a,b**). Because within-reviewer variance was lower than the pooled variance, quantitative data from a single reviewer (AN) were used for all figures and tables. Pooled vs. single-reviewer analysis had no impact on statistical significance or the overall magnitude of changes observed. Global LV contractile function and regional wall thickness data were computed from the short-axis cine images. LV endocardial boundaries were traced at end-diastole and end-systole using standard cardiac analysis software (Intellispace Portal, Philips, Best, Netherlands) to obtain end-systolic, end-diastolic volume, LV myocardial mass (LVmass), stroke volume (difference between end-diastolic and end-systolic volumes), cardiac output (CO), and LV ejection fraction (LVEF). LVEF was calculated as the ratio of stroke volume to end-diastolic volume. Papillary muscles were excluded from the volume calculations. Left ventricle wall thickening (LVTh) was calculated as relative difference in LV wall thickness in end-systole and end-diastole, divided by end-diastolic thickness. LVTh was evaluated at the infarcted and non-infarcted areas of the each slice of the heart. Infarct size was calculated from delayed Gd-enhanced images and presented as the ratio of scar area to total LV area.

Echocardiography. Baseline transthoracic echocardiography was performed before infarct surgery to evaluate the animals' cardiac function. Macaques were sedated with ketamine and propofol and then were examined in the supine position, using a commercially available ultrasound system with a 5 MHz probe (Vivid-q, GE Healthcare, Horten, Norway). Apical four-chamber views were collected for baseline left ventricular ejection fraction (LVEF) measurement. Quantification of LVEF was performed by a qualified cardiologist according to the recommendation of the American Society of Echocardiography.

Telemetric EKG. EKG recordings were acquired from conscious, freely mobile animals using a Vmed Vetcheck telemetry system. Animals had tunneled subcutaneous EKG wires implanted, providing lead II tracings. Continuous telemetry was sent wirelessly to a dedicated laptop for all macaques with myocardial infarction with or without hESC-CM delivery on post-myocardial infarction days 1, 4, 7, 10, and 13 and post-intramyocardial injection days 3, 6, 9, 12, 15, 18, 21, 24, and 27. All EKG traces were evaluated manually by a cardiologist (Y.-W.L.) using EKG Reviewer (Vmed), and the total number and duration of ventricular arrhythmias determined. A second cardiologist (B.C.) evaluated a subset of these telemetry tracings in a blinded manner, with excellent concordance (**Supplementary Fig. 3c**). Premature ventricular complexes (PVCs) were defined as QRS complexes greater than 60 ms. Ventricular tachycardia (VT) was defined as a run of four or more PVCs with ventricular rate of more than 180 beats per min. Accelerated idioventricular rhythm (AIVR) was defined as four or more PVCs with a rate of less than 180 beats per min. VT or AIVR were considered sustained if the duration was greater than 30 s.

Histology and immunohistochemistry. Histological studies were carried out as detailed previously[19,25] with some adaptation. Paraformaldehyde-fixed macaque hearts were dissected to remove the atria and right ventricle before cross-sections were obtained by sectioning parallel to the short axis at 2.5 mm thickness on a commercial slicer (Berkel). Weights of the whole heart, left ventricle, and each slice were obtained before cutting heart slices to fit tissue cassettes. The tissue then was processed and embedded in paraffin, and four-micrometer sections were cut for staining. For morphometry, infarct regions were identified by Picrosirius red staining; human grafts were identified by anti-human cardiac troponin I, stained using avidin-biotin reaction (ABC kits from VectorLabs) followed by chromogenic detection via diaminobenzidine (Sigmafast, Sigma Life Science). The slides were digitized using a Hamamatsu Nanozoomer whole slide scanner, and the images were viewed and exported with NDP software (NDP.view 2.6.13). Resulting images were imported into Image J software (version 1.51 k) where area of infarct and graft (region of interest or ROI) were measured. The mass of the ROI was determined by calculating the ratio of ROI area to total tissue area on the slide, and multiplying by the weight of the tissue the slide was cut from. The entire scar or graft was expressed as total weight or percent of LV mass.

For immunohistochemistry, we used the primary antibodies listed in **Supplementary Table 2**. Primary antibodies then were followed either with fluorescent secondary antibodies (Alexa-conjugated, species-specific antibodies from Molecular Probes) or the avidin biotin reaction (ABC kits from VectorLabs), followed by chromogenic detection via diaminobenzidine (Sigmafast, Sigma Life Science). Immunofluorescent images were collected with either a Nikon A1Confocal System or a Nikon Ti-E inverted widefield microscope. For high-resolution confocal images, a 60× CFI Plan Apo Water immersion objective lens (NA 1.2) was used. 12-bit images were captured with the pinhole at 1 Airy Unit and field size at 1,024 × 1,024 pixels. For large field immunostained sections, a CFI Pan Apo lambda 4× objective (NA 0.2) was used on the widefield system. Grids of 14-bit Images were captured using a Photometrics CoolSnap HQ2 CCD camera and stitched with NIS Elements version 5.00 software. For figure preparation, images were exported into Photoshop CS3 (Adobe). If necessary, brightness and contrast were adjusted for the entire image and the image was cropped.

Histomorphometry. Infarct size was determined from whole-slide scans of picrosirius red-fast green stained tissue sections. Infarct size was calculated as Σ(block mass × infarct area/block area) and expressed as a percentage of the left ventricular mass.

Graft size was determined from whole-slide scans of sections stained with human-specific cTnT. Graft size was calculated as Σ(block mass × graft area/block area) and expressed either as a percentage of the left ventricular mass or the infarct mass.

Vascular density was determined from photomicrographs of CD31-stained sections from the graft, scar, and remote (non-infarcted) myocardium obtained with a 40× objective. A defined-area grid was overlaid onto the image, and vascular profiles within a region of interest were counted. Vessels that crossed into multiple grid subunits were counted only once. Vascular density is expressed as the number of vessels/mm².

Graft cardiomyocyte number was estimated from photomicrographs of sections stained with pericentriolar material-1 (PCM-1). Regions of interest shown to contain no host cardiomyocytes in adjacent sections were photographed with a 40× objective. A defined-area grid was overlaid onto the image, and PCM-1⁺ nuclear profiles with clear rings of perinuclear staining were counted. To determine the number of microscopic fields required, we performed a systematic downsampling study. Counting 42, 25, 10, and 5 fields yielded cardiomyocyte densities of 3,865, 3,848, 3,934, and 3,858 nuclei/mm². Subsequent studies were done with five fields per heart. To calculate graft cardiomyocyte nuclear density on a volume basis, we made the assumption that the nuclei were isotropically packed, that is, that the densities in the XY, XZ, and YZ planes were equivalent. (This was supported by microscopic observation that linear nuclear densities in the X and Y dimensions were comparable.) Volume-based nuclear density was calculated as $(\text{nuclei/mm}^2)^{1.5}$, yielding nuclei/mm³. Finally, because our grafts were relatively immature, we made the assumption that each cardiomyocyte was mononucleated, meaning that nuclear density = cardiomyocyte density. (Note that even in adult human myocardium, only 25% of cardiomyocytes have more than one nucleus[2], so the impact of this assumption is modest.) Total graft number was determined as:

$$\text{total graft cardiomyocyte number} = \frac{\text{graft cardiomyocyte number}}{\text{mm}^3} \times \frac{\text{graft mass(mg)}}{\text{tissue density}\left(1.06\frac{\text{mg}}{\text{mm}^3}\right)}$$

The proliferation rate of engrafted cardiomyocytes was determined from sections stained for PCM-1 and Ki67. Regions of interest shown to contain no host cardiomyocytes in adjacent sections were photographed with a 40× objective. Cardiomyocyte nuclei were identified by a clear perinuclear ring of PCM-1 staining. The number of cells counted ranged from 607 to 1,341 per heart. The proliferation rate is expressed as 100×(the number of PCM-1⁺/Ki67⁺ double-positive nuclei) divided by the number of PCM-1⁺ nuclei.

In situ hybridization. Engrafted human cells were identified using *in situ* hybridization with a human-specific pan-centromeric genomic probe as previously reported[4] and used to validate human specific antibodies. In brief, the human-specific pan-centromeric probe was generated by modification of a protocol previously reported[7] that involves degenerate PCR with primers against human alpha satellite pan-centromeric repeat sequences. PCR was performed for 30 cycles: denaturation at 94 °C for 1 min; annealing at 45 °C for 1 min; extension at 72 °C for 1 min. We then labeled the PCR product with biotin (Biotin DecaLabel DNA kit, Thermo Scientific) to generate the *in situ* probe. The pan-centromeric probe was diluted in hybridization buffer (0.5× SSC, 10% dextran sulfate, 50% deionized formamide, 0.4 mg/mL salmon sperm DNA), heated to 80 °C to denature the DNA, applied to the slide and hybridized overnight at 37 °C. Subsequent detection after *in situ* hybridization used peroxidase-conjugated avidin (ABC kits from VectorLabs). For immunohistochemistry, the *in situ* probe was detected by Alexa Fluor 594 tyramide amplification (Molecular Probes).

PCR detection of human DNA. One of the hESC-CM-treated animals had a renal tumor identified during necropsy. Human- and macaque-specific primers were used to determine that the tumor was not human tissue. Genomic DNA was isolated from adjacent slices (with respect to pan-centromeric probe section) using a Qiagen DNeasy tissue kit and 250 ng of input gDNA per sample was used for PCR. Human (HS) and macaque (MN) gDNA was used as controls.

To detect human DNA, we made primers targeting human mitochondria: forward primer 5′-CACCGGCGCAGTCATTCTCATA-3′ and reverse primer 5′-GAGTCCTGTAAGTAGGAGA-3′. PCR profile: 95 °C/1 min, 59 °C/1 min, 72 °C/1 min for 40 cycles, product size 267 bp. Human-specific primers detect a 249 bp region on human mitochondria DNA (11680–11929; MF992925.1).

For macaque-specific PCR, we developed primers targeting chromosome-3: forward primer 5′-CAGTTGGCTGTTCAGTATAGCGAT-3′ and reverse primer 5′-CTTCAGAGTATGTGACATAGGT-3′. PCR profile: 95 °C/1 min, 55 °C/1 min, 72 °C/1 min for 40 cycles, product size 150 bp. Macaque-specific

primers detect a 150 bp region on macaque chromosome 3 (8392421–8392571; LT160002.1).

Electrophysiology studies. To determine inducibility and mechanism of ventricular arrhythmias, macaques underwent catheter-based electrophysiology study. The animals were sedated with ketamine and propofol and intubated. Anesthesia was maintained with sevoflurane. Heart rate, non-invasive blood pressure, and pulse oximetry monitors were connected. R2 pads were placed and connected to a defibrillator. Depending upon the animal and prior vascular access, either the left or right femoral artery was accessed using a hybrid cut down/Seldinger technique. A 7 French hemostatic sheath was placed into the femoral artery. Through this sheath a CARTO NaviStar B-curve, D-curve, or a PENTARAY (Biosense Webster Inc., Diamond Bar, CA) catheter was placed and advanced retrograde through the aortic arch into the left ventricle. If the macaque was in sinus rhythm at the onset of the study, a substrate map was created in sinus rhythm and areas of low voltage annotated. Scar was defined as a voltage of <0.5 mV and/or inability to capture the myocardium at a pacing output of 10 mA at 2 ms pulse width. Diseased myocardium was defined by a voltage of 0.5–1.5 mV, and healthy myocardium >1.5 mV. Following substrate mapping, a ventricular stimulation protocol was performed with an 8-beat drive train with single, double, and triple extrastimuli down to the ventricular effective refractory period. The protocol was repeated at two sites and two drive-train cycle lengths. If non-inducible under baseline conditions, the protocol was repeated on an isoproterenol infusion titrated to achieve a 25% increase in baseline heart rate. Inducibility and severity were graded using the scales presented in **Supplementary Tables 3** and **4**.

For induced and spontaneous ventricular arrhythmias, electroanatomic and voltage mapping was performed. The arrhythmia was characterized as focal if there was radial spread of electrical activation from a point source and macro-reentrant if there was an identified circuit of electrical activity with an early-meets-late activation pattern. Activation mapping was performed using the CARTO III system with either a 7-French NaviStar B- or D-curve catheter or a 7-French D-curve PENTARAY catheter (Biosense Webster Inc, South Diamond Bar, CA, USA).

Statistical analysis. All values are expressed as mean ± s.e.m. Paired *t*-tests and two-tailed *t*-tests were performed using Graphpad Prism software, with the threshold for significance level set at $P < 0.05$.

Life Sciences Reporting Summary. Further information on experimental design is available in the Nature Research Reporting Summary linked to this article.

Data availability. Additional information from the study is available from the corresponding author murry@uw.edu upon request.

46. Fernandes, S. *et al.* Human embryonic stem cell-derived cardiomyocytes engraft but do not alter cardiac remodeling after chronic infarction in rats. *J. Mol. Cell. Cardiol.* **49**, 941–949 (2010).

nature research

Corresponding author(s): Charles E. Murry

Reporting Summary

Nature Research wishes to improve the reproducibility of the work that we publish. This form provides structure for consistency and transparency in reporting. For further information on Nature Research policies, see Authors & Referees and the Editorial Policy Checklist.

Statistical parameters

When statistical analyses are reported, confirm that the following items are present in the relevant location (e.g. figure legend, table legend, main text, or Methods section).

n/a	Confirmed	
☐	☒	The exact sample size (*n*) for each experimental group/condition, given as a discrete number and unit of measurement
☐	☒	An indication of whether measurements were taken from distinct samples or whether the same sample was measured repeatedly
☐	☒	The statistical test(s) used AND whether they are one- or two-sided *Only common tests should be described solely by name; describe more complex techniques in the Methods section.*
☐	☒	A description of all covariates tested
☐	☒	A description of any assumptions or corrections, such as tests of normality and adjustment for multiple comparisons
☐	☒	A full description of the statistics including central tendency (e.g. means) or other basic estimates (e.g. regression coefficient) AND variation (e.g. standard deviation) or associated estimates of uncertainty (e.g. confidence intervals)
☐	☒	For null hypothesis testing, the test statistic (e.g. *F*, *t*, *r*) with confidence intervals, effect sizes, degrees of freedom and *P* value noted *Give P values as exact values whenever suitable.*
☐	☒	For Bayesian analysis, information on the choice of priors and Markov chain Monte Carlo settings
☐	☒	For hierarchical and complex designs, identification of the appropriate level for tests and full reporting of outcomes
☐	☒	Estimates of effect sizes (e.g. Cohen's *d*, Pearson's *r*), indicating how they were calculated
☐	☒	Clearly defined error bars *State explicitly what error bars represent (e.g. SD, SE, CI)*

Our web collection on statistics for biologists may be useful.

Software and code

Policy information about availability of computer code

Data collection	• Echocardiography was done using a commercially available ultrasound system with a 5 MHz probe (Vivid-q, GE Healthcare, Horten, Norway). • EKG recordings were acquired using a Vmed Vetcheck telemetry system. • Hamamatsu Nanozoomer whole slide scanner was used to get the whole slide images. The images from the scanner is viewed with NDP software (NDP.view 2.6.13). • Microscopic histological images were taken using NIS Elements Version 5.00. • Activation mapping was performed using the CARTO III system with either a 7-French NaviStar B- or D-curve catheter or a 7-French D-curve PENTARAY catheter (Biosense Webster Inc, South Diamond Bar, CA, USA)
Data analysis	• Statistical analysis was performed using Graphpad Prism software version 7. • The images from Hamamatsu Nanozoomer whole slide scanner is viewed with NDP software (NDP.view 2.6.13). • Image J (version 1.51s) was used to view and adjust brightness/contrast of the histological images. • Histological images were taken using NIS Elements Version 5.00. • Cardiac MRI analysis was done using Intellispace Portal version 9.0, Philips, Best, Netherlands.

For manuscripts utilizing custom algorithms or software that are central to the research but not yet described in published literature, software must be made available to editors/reviewers upon request. We strongly encourage code deposition in a community repository (e.g. GitHub). See the Nature Research guidelines for submitting code & software for further information.

Data

Policy information about availability of data

All manuscripts must include a data availability statement. This statement should provide the following information, where applicable:

- Accession codes, unique identifiers, or web links for publicly available datasets
- A list of figures that have associated raw data
- A description of any restrictions on data availability

> This study did not generate genomic data sets. Most of the data associated with the study have been included in the main figures and table, or the supplementary figures and tables. Any other datasets generated during and/or analysed during the current study are available from the corresponding author on reasonable request.

Field-specific reporting

Please select the best fit for your research. If you are not sure, read the appropriate sections before making your selection.

☒ Life sciences   ☐ Behavioural & social sciences   ☐ Ecological, evolutionary & environmental sciences

For a reference copy of the document with all sections, see nature.com/authors/policies/ReportingSummary-flat.pdf

Life sciences study design

All studies must disclose on these points even when the disclosure is negative.

Sample size	Our principal endpoint was ejection fraction, determined by MRI. We performed a power analysis using pilot data from infarcted animals. This showed we could detect a 25% increase in ejection fraction with an alpha of 0.05 and a beta of 0.8 using group sizes of 4.
Data exclusions	Several animals were excluded due to complications leading to early euthanasia. The flow chart including every enrolled animal and its fate is presented in Suppl. Fig. 2.
Replication	The nature of primate work does not readily lend itself to doing multiple batches of experiments. We continuously enrolled animals over a 4-year period to complete this project. The results were quite consistent from animal to animal.
Randomization	The animals were not randomized due to the complexities of having a 4-person cell preparation team come in early on the mornings of cell transplantation experiments. We enrolled approximately twice as many cell-treated animals as controls, due to the need to study the arrhythmias induced by the cell transplantation.
Blinding	The MRI scans were performed and evaluated by 3 investigators who were blinded to treatment. There was excellent inter-observer variability. The electrophysiology analyses were performed and analyzed principally by one investigator who was blinded to treatment. A subset of his analyses were repeated by a second blinded reviewer, and there was excellent inter-observer variability.

Reporting for specific materials, systems and methods

Materials & experimental systems

n/a	Involved in the study
☒	☐ Unique biological materials
☐	☒ Antibodies
☐	☒ Eukaryotic cell lines
☒	☐ Palaeontology
☐	☒ Animals and other organisms
☒	☐ Human research participants

Methods

n/a	Involved in the study
☒	☐ ChIP-seq
☐	☒ Flow cytometry
☒	☐ MRI-based neuroimaging

Antibodies

Antibodies used	The following data are presented in a more legible format in Supplementary Table 2. Antigen Antibody type Company Catalog # Lot # Dilution cTnI Rabbit monoclonal Abcam Ab52862 GR116627-7 and GR116627-10 1:200 ssTnI Mouse monoclonal Novus NBP2-46170 F001 1:200

cTnT Mouse monoclonal Invitrogen MA5-12960 SH2439467A 1:100
Collagen 1 Goat polyclonal Abcam Ab24821 GR3175980-1 1:200
MLC2a Mouse monoclonal Becton-Dickinson 565496 5082617 1:500
MLC2v Rabbit polyclonal Proteintech 10906-1-AP 39557 1:100
Cav 3 Rabbit polyclonal Abcam Ab2912 GR2939265 1:200
Pan-cadherin Rabbit polyclonal Sigma C3678 030M4772 1:100
Connexin 43 Rabbit polyclonal Sigma C6219 045M4882V 1:200
Desmin Goat polyclonal Santa Cruz Sc-7559 G1014 1:50
CD31 Mouse monoclonal Abcam Ab9498 GR3192748-2 1:20
PCM-1 Rabbit polyclonal Sigma HPA023370 GR304183-6 1:100
Ki67 Mouse monoclonal BD Bioscience BDB558615 7242989 1:20

Validation	Each antibody was validated using established positive and negative controls and titered for an optimal signal:noise ratio. Both human and macaque monkey samples were used to establish which antibodies to use and the specifics of their immunostaining assays.

Eukaryotic cell lines

Policy information about cell lines

Cell line source(s)	We used RUES2 (Rockefeller University) and H7 (University of Wisconsin/WiCell) human embryonic stem cell lines.
Authentication	We used a commercial short tandem repeat assay and matched our results against published standards for both cell lines.
Mycoplasma contamination	All cells were routinely tested for mycoplasma and were negative.
Commonly misidentified lines (See ICLAC register)	Neither of our cell lines are on the ICLAC registry.

Animals and other organisms

Policy information about studies involving animals; ARRIVE guidelines recommended for reporting animal research

Laboratory animals	The subjects in our study were pigtailed macaques, Macaca nemestrina. They were provided by the Washington National Primate Research Center. Both male and female animals were studied. Specific details on gender, age, weight are pasted below. They also can be found in Table 1 of the manuscript in a more legible format. Control P14 M 6y 10mo 12.6 P15 F 9y 7mo 11.7 P18 F 10y 9mo 11.4 P20 F 6y 0mo 10.6 Mean 8 11.6 SEM 1 0.4 hESC-CM P22 F 15y 7mo 7.0 P23 F 11y 6mo 10.7 P24 F 12y 2mo 9.5 P25 F 6y 7mo 5.2 P39 F 14y 6 mo 9.2 Mean 11 8.6 SEM 2 0.9
Wild animals	The study did not involve wild animals.
Field-collected samples	The study did not involve samples collected from the field.

Flow Cytometry

Plots

Confirm that:

☒ The axis labels state the marker and fluorochrome used (e.g. CD4-FITC).

☒ The axis scales are clearly visible. Include numbers along axes only for bottom left plot of group (a 'group' is an analysis of identical markers).

☒ All plots are contour plots with outliers or pseudocolor plots.

☒ A numerical value for number of cells or percentage (with statistics) is provided.

Methodology

Sample preparation	Cardiomyocytes derived from Rues or H7 embryonic stem cells were dissociated into single cells by consecutive treatment of Liberase TH solution (ROCHE, cat. 5401151001) and TryPLE (ThermoFisher, cat. A1285901) and fixed by 4% paraformaldehyde and incubated with a mouse monoclonal cTnT antibody (clone 1C11, Abcam, cat. ab8295) and isotype control (mouse IgG1, kappa antibody clone B11/6, Abcam, cat. ab91353), followed by incubation with an PE-conjugated goat anti-mouse secondary antibody.
Instrument	BD Accuri C6
Software	BD Accuri C6 software, version 1.0. 264.21
Cell population abundance	Cell populations that had 86 to 98.7% cTnT-positive cardiomyocytes were used for transplantation.
Gating strategy	a) The major cell population which was considered as single cells was gated from forward scatter/side scatter plot of isotype staining. b) The PE channel of the isotype control was gated at approximately 1.0% to be used for cTnT-positive cell gating. c) Use the gating of isotype control to determine population size of cTnT-positive cells.

☒ Tick this box to confirm that a figure exemplifying the gating strategy is provided in the Supplementary Information.

nature research

Corresponding author(s):   Murry C.E.

☐ Initial submission   ☐ Revised version   ☒ Final submission

MRI Studies Reporting Summary

Form fields will expand as needed. Please do not leave fields blank.

▶ Experimental design

1. Describe the experimental design.

Cardiac MRI was performed prior to cell injection (2 weeks after myocardial infarction) and at 4 week and 12 week post cell-injection. In vivo imaging studies were conducted on a 3-Tesla Achieva clinical scanner (Philips, Best, Netherlands). Depending on the animal size, two overlapped Flex-M and Flex-L coils (dual-element, approximately 15 and 20 cm diameter, respectively) or an 8-element knee coil was used. Pediatric ECG leads were used for gating of MRI acquisitions. ECG, respiration rate, arterial oxygen saturation and body temperature were monitored continuously.

2. Specify the number of blocks, trials or experimental units per session and/or subject, and specify the length of each trial or block (if trials are blocked) and interval between trials.

One animal was scanned in each imaging session. Length of each imaging session was about 2 hours.

3. Describe how behavioral performance was measured.

N/A.

▶ Acquisition

4. Imaging

   a. Specify the type(s) of imaging.

   Structural and functional imaging of the heart.

   b. Specify the field strength (in Tesla).

   3 Tesla

   c. Provide the essential sequence imaging parameters.

   CINE images were acquired with a RF-spoiled turbo field echo (T1-TFE) sequence that generated 25-30 cardiac phases for 10-12 short axis slices spanning the left ventricle. Acquisition parameters included a repetition time (TR) 3.9 msec, echo time (TE) 1.9 msec, a 15° flip angle (FA), 4 mm slice thickness (no gap), field of view (FOV) 120x120 mm2, 1 mm2 voxel size, 6-8 signal averages, retrospective ECG gating without breath hold.

   Animals subsequently received an intravenous bolus injection of gadolinium-based contrast agent ProHance (Bracco Diagnostics Inc., Princeton, NJ) 0.2 mmol/kg, followed by a saline flush. At 8 minutes after injection, TI-scout images were acquired for determination of inversion time (TI) to null signal from non-infarcted myocardium. At nine minutes post-injection of contrast agent, phase-sensitive inversion recovery (PSIR) multislice images were acquired at the LV short axis to visualize infarct: TR/TE 7.3/3.5 msec, FA 25°, voxel size 1.3 mm2, FOV 150x150 mm2, slice thickness 4 mm without gap, four averages. This was repeated in the long axis plane. Inversion time range 280-350 msec, adjusted by the operator based on TI-scout values.

   d. For diffusion MRI, provide full details of imaging parameters.

   N/A.

5. State area of acquisition.

   Heart.

▶ Preprocessing

6. Describe the software used for preprocessing.	A standard Philips Intellispace Portal software version is v7.0.1.20482 was used for cardiac analysis (Best, Netherlands).

7. Normalization

a. If data were normalized/standardized, describe the approach(es).	N/A.
b. Describe the template used for normalization/ transformation.	N/A.

8. Describe your procedure for artifact and structured noise removal.	ECG gating was complicated by a weak signal and presence of arrhythmias in some infarcted animals. Prospective ECG triggering was used when retrospective gating was not successful or if the scan was abrupted due to arrhythmia. Respiratory gating was not used because of the absence of the plateau segments in respiration waves. No mechanical respiration devices were used. Respiratory motion was noticeable in imaging, but not critical to image quality. Blood flow artifacts are common in the infarcted animals. Blood flow correction techniques are not always effective in fast heart rates.
9. Define your software and/or method and criteria for volume censoring, and state the extent of such censoring.	N/A.

▶ Statistical modeling & inference

10. Define your model type and settings.	Univariate and multivariate statistics were used.
11. Specify the precise effect tested.	Paired t-test statistical method was used to compare means for the same studied animals imaged in different time points. For comparison of two means of the different studied groups, a t-test assuming unequal variances was used. One-way ANOVA was used to test the difference in left ventricle dimensions and contractile function between control and cell-treated group. The differences were considered statistically significant with p value less than 0.05.

12. Analysis

a. Specify whether analysis is whole brain or ROI-based.	Whole heart analysis.
b. If ROI-based, describe how anatomical locations were determined.	Regional left ventricle wall thickness in end-systole and end-diastole was measured from CINE images in three infarcted slices in the middle of the infarcted area and a border zone and then averaged. Extension of the infarcted zone was determined from the late gadolinium enhanced images.

13. State the statistic type for inference. (See Eklund et al. 2016.)	N/A.
14. Describe the type of correction and how it is obtained for multiple comparisons.	N/A.

15. Connectivity

a. For functional and/or effective connectivity, report the measures of dependence used and the model details.	N/A.
b. For graph analysis, report the dependent variable and functional connectivity measure.	N/A.

16. For multivariate modeling and predictive analysis, specify independent variables, features extraction and dimension reduction, model, training and evaluation metrics.

Erratum: Human embryonic stem cell–derived cardiomyocytes restore function in infarcted hearts of non-human primates

Yen-Wen Liu, Billy Chen, Xiulan Yang, James A Fugate, Faith A Kalucki, Akiko Futakuchi-Tsuchida, Larry Couture, Keith W Vogel, Clifford A Astley, Audrey Baldessari, Jason Ogle, Creighton W Don, Zachary L Steinberg, Stephen P Seslar, Stephanie A Tuck, Hiroshi Tsuchida, Anna V Naumova, Sarah K Dupras, Milly S Lyu, James Lee, Dale W Hailey, Hans Reinecke, Lil Pabon, Benjamin H Fryer, W Robb MacLellan, R Scott Thies & Charles E Murry

In the version of this article initially published, NIH grant P51 OD010425 was omitted. The error has been corrected in the HTML and PDF versions of the article.